INFN/TC-00/17
9 Settembre 2000

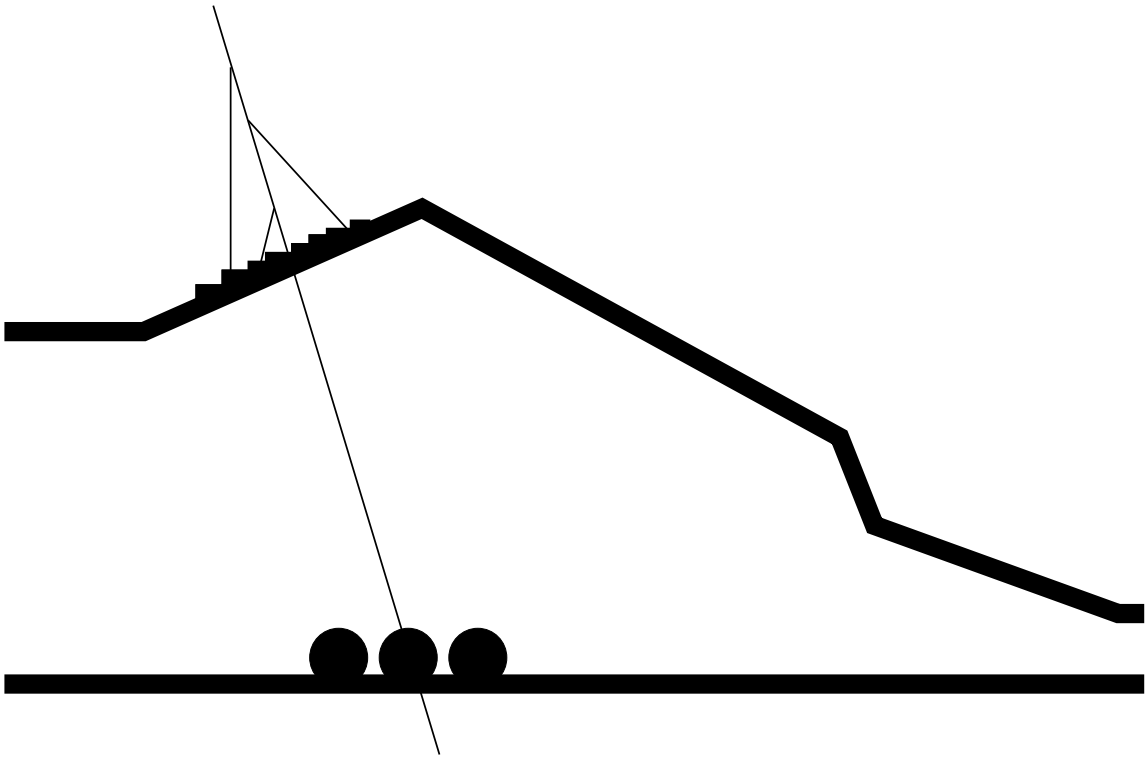

Resolutions of a large volume liquid scintillator detector

O.Ju.Smirnov[a]

INFN - Laboratori Nazionali del Gran Sasso

INFN - Istituto Nazionale di Fisica Nucleare
Laboratori Nazionali del Gran Sasso

INFN/TC-00/17
9 Settembre 2000

Resolutions of a large volume liquid scintillator detector

O.Ju.Smirnov[a]

[a] *Joint Institute for Nuclear Research, Dubna, Russia*

Abstract

The energy and spatial resolutions of a large volume liquid scintillator detector with a spherical symmetry are discussed in detail. An event reconstruction technique using charge and time data from the PMTs is analysed in order to obtain optimal detector resolutions. The relations for the numerical estimations of the energy and spatial resolutions are obtained and verified with the CTF detector data.

The list of the notations and abbreviations used in the article:

N_{PM} total number of the PMTs of the detector;

Q total charge registered by the detector;

$\mu_0 = \frac{Q}{N_{PM}}$ mean charge registered by the one PMT of the detector;

μ_i the mean charge registered by the i-th PMT of the detector;

$s_i = \frac{\mu_i}{\mu_0}$ sensitivity of the i-th PMT;

$v_1 = (\frac{\sigma_{\mu_1}}{\mu_1})^2$ relative variance of the single photoelectron spectrum;

$f(\overrightarrow{r})$ geometrical function of the detector that relates the charge registered by a PMT for the source at position with coordinates $\overrightarrow{r}$ to the charge, registered by the same PMT for the same source positioned at the detector's center. Coordinates $\overrightarrow{r}$ are the source coordinates in the PMT coordinate system;

$f_s(\overrightarrow{r})$ geometrical factor of the detector that relates the charge registered by a detector for the source at position with coordinates $\overrightarrow{r}$ to the charge, registered by the detector for the same source positioned at the detector's center. Coordinates $\overrightarrow{r}$ are the source coordinates in the detector coordinate system;

PMT- photoelectron multiplier tube;

CTF- counting test facility of the Borexino detector;

SER- single electron response (charge spectrum corresponding to a single photoelectron);

p.e.- photoelectron.

1 Introduction

The energy resolution of the scintillator detector has been studied during the early years of the scintillation detectors development. A good review of the scintillation technique can be found in [1]. The spatial and energy resolutions of recently constructed large volume liquid scintillator detectors is being studied with Monte-Carlo simulations (see i.e. [2]). In the present article some relations are obtained that provide numerical estimations of the energy and spatial resolution of a large volume liquid scintillator detector with a spherical symmetry. The data of the CTF detector [3] are used to check the validity of the estimations. Some predictions for the resolution of the Borexino detector [2] are presented as well.

Let us give a reminder of some fundamental relations from PMT operation theory. The relative variance of a PMT charge response can be written using the relative variance of the single photoelectron response $v_1 = (\frac{\sigma_{\mu_1}}{\mu_1})^2$ of the PMT, and the mean number of photoelectrons (p.e.) μ registered in a scintillation event (see i.e. [1])

$$v \equiv \left(\frac{\sigma_\mu}{\mu}\right)^2 = \frac{1+v_1}{\mu}. \tag{1}$$

Here the normal distribution of the amount of light emitted in a scintillation event is assumed.

The physical meaning of equation (1) is straightforward. If $v_1 \to 0$ (as for a delta-function response of a PMT) then the relative variance of a PMT response is that of a Poisson distribution ($\frac{1}{\mu}$) of the registered number of p.e. This relation gives a fundamental limit for the PMT energy resolution. So the only way to improve the PMT energy resolution is to make the SER more "sharp". The PMT energy resolution is frequently characterised in literature by the so called peak-to-valley ratio, but this value can't be used for direct numerical estimations. Indeed, one can consider two PMTs with the same peak-to-valley ratio but with a different distribution of high amplitude events in the "tail" of SER. These PMTs will have different single p.e. relative variances and hence different energy resolutions, but one can't realize it from the peak-to-valley ratio.

More detailed considerations of the practical scintillation counter lead to different equations for the PMT signal relative variance, such as ([1]):

$$v = v(p) + \frac{1+v_1}{\mu}. \tag{2}$$

Here the parameter $v(p)$ takes into account all the possible ways the photon can arrive at the PMT photocathode, and all the possible fluctuations in the process of its registration.

2 Energy resolution

2.1 The energy resolution for a monoenergetic point-like source at the detector's center

Let us consider a monoenergetic point-like source at a detector's center. The total signal of the detector is the convolution of the signals from the PMTs; this means the total signal variation is the sum of the variations of the PMTs:

$$\sigma_{Q_0}^2 = \sum_i^{N_{PM}} \sigma_{\mu_i}^2 = \sum_i^{N_{PM}} \mu_i(1+v_{1_i}) = Q_0 \cdot (1 + \frac{1}{N_{PM}} \sum_i^{N_{PM}} s_i v_{1_i}) = Q_0 \cdot (1 + v_1^{Det}(0)) \,, \quad (3)$$

where:

$$v_1^{Det}(0) = \frac{1}{N_{PM}} \sum_i^{N_{PM}} s_i v_{1_i} \,. \quad (4)$$

The mean value of the total charge Q_0 is the sum of the mean signals from the PMTs:

$$Q_0 = \sum_i^{N_{PM}} \mu_i \,.$$

So the energy resolution for the source at the detector's center is:

$$R(Q,0) \equiv \sqrt{\frac{\sigma_{Q_0}^2}{Q_0^2}} = \sqrt{\frac{1 + v_1^{Det}(0)}{Q_0}} \,. \quad (5)$$

One can see that the detector's energy resolution behaves in the same way as for the energy resolution of a single PMT (1), with the parameter v_1 replaced by the average parameter $v_1^{Det}(0)$ that also takes into account the different relative sensitivities of the PMTs.

2.2 The energy resolution for a monoenergetic point-like source not at the detector's center

Let us consider now a source at an arbitrary position in the detector. The mean charge registered by the $i-th$ PMT can be recalculated from the known registered charge for the same source at the detector's center:

$$\mu_i(\overrightarrow{r_i}) = \mu_{0_i} \cdot f(\overrightarrow{r_i}) = \mu_0 \cdot s_i \cdot f(\overrightarrow{r_i}) \,. \quad (6)$$

Here $\overrightarrow{r_i}$ are the source coordinates in the i-th PMT coordinate system and s_i is the relative sensitivity of the i-th PMT. Because of the detector's spherical symmetry it is

Figure 1: The coordinate system: the event occurs at the point with coordinates (r, Θ) in the coordinate system of the chosen PMT (X-axis of the coordinates system passes from the detector's center to the PMT). Because of the detector's spherical symmetry the event in the i-th PMT coordinate system is characterized by another couple of polar coordinates $\{\mathrm{r},\Theta_i\}$. Since the spatial coordinates of all the PMTs in the detector are fixed, then the position of the source in the coordinates system of any PMT can be easily calculated.

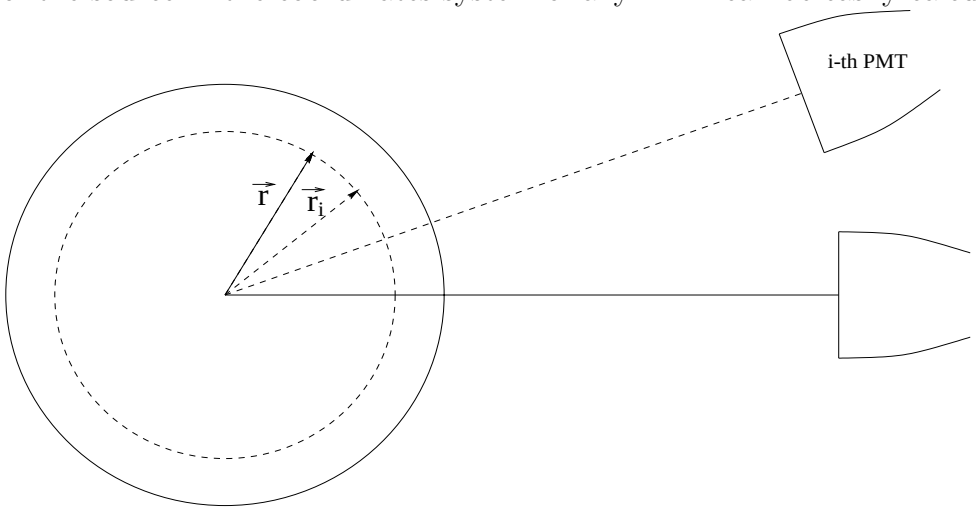

convenient to use a geometrical function $f(\overrightarrow{r})$ in the coordinate system related to the PMT (the X-axis passes from the detector's center to the PMT as shown in fig.1). The geometrical function depends only on the distance from the source to the detector's center r and the azimuthal angle Θ (where angle the Θ is calculated from the X-axis passing from the detector's center to the PMT):

$$f(\overrightarrow{r}) = f(r, \Theta)\,. \tag{7}$$

The independence of the geometrical function from the source energy is assumed in (6).

As before, the total signal of the detector is the convolution of the PMT signals. Hence the mean value $Q(\overrightarrow{r})$ of the total signal is the sum of the mean values for all the PMTs, and the variance $\sigma_Q^2(\overrightarrow{r})$ is the sum of the variances for all the PMTs :

$$Q(\overrightarrow{r}) = \sum_i^{N_{PM}} \mu_i(\overrightarrow{r_i}) = \sum_i^{N_{PM}} \mu_0 \cdot s_i \cdot f(\overrightarrow{r_i}) = Q_0 \frac{1}{N_{PM}} \sum_i^{N_{PM}} s_i \cdot f(\overrightarrow{r_i}) = Q_0 \cdot f_s(\overrightarrow{r})\,, \tag{8}$$

$$\sigma_Q^2(\overrightarrow{r}) = \sum_i^{N_{PM}} \sigma_{\mu_i}^2(\overrightarrow{r_i}) = \sum_i^{N_{PM}} \mu_i(\overrightarrow{r_i})(1 + v_{1_i}) =$$

$$= Q_0 \cdot f_s(\overrightarrow{r}) + Q_0 \frac{1}{N_{PM}} \sum_i^{N_{PM}} s_i \cdot f(\overrightarrow{r_i}) \cdot v_{1_i})\,, \tag{9}$$

where:

$\overrightarrow{r}$ are the coordinates of the source in the detector's coordinate system;

$\overrightarrow{r}_i$ are the coordinates of the source in the i-th PMT coordinate system;

Q_0 is the total charge registered by the detector for the same source positioned at the detector's center;

$f_s(\overrightarrow{r})$ is a geometrical function of the detector that relates the charge registered by a detector for the source at position with coordinates $\overrightarrow{r}$ to the charge, registered for the same source positioned at the detector's center. Coordinates $\overrightarrow{r}$ are the source coordinates in the detector coordinate system.

The factor $f_s(\overrightarrow{r})$ is related to the geometrical function $f(\overrightarrow{r})$ defined by (6) in the following way:

$$f_s(\overrightarrow{r}) \equiv \frac{1}{N_{PM}} \sum_{i}^{N_{PM}} s_i \cdot f(\overrightarrow{r_i}) \simeq \frac{1}{2} \int_0^{\pi} f(r, \Theta) \sin(\Theta)\, d\theta\,. \tag{10}$$

Here an approximate equality is used to underline the approximate nature of the passing from the summation over PMTs to the integration of the continuous function. The ideal spherical symmetry of the detector is assumed here, which is not precisely the case because of the different sensitivities of the PMTs and the nonuniform PMT distribution over the spherical surface. The modeling of the CTF detector shows that up to $r = 50 - 60$ cm the equality is satisfied within the precision of calculations. At bigger r the deviation doesn't exceed $1 - 2\%$ percent, and the deviation depends on the source position. Let us notice that:

- $f(\overrightarrow{r})$ is a single PMT function;
- $f_s(r)$ is the detector's function.

Let us introduce a parameter of the detector $v_1^{Det}(\overrightarrow{r})$, corresponding to (4) for a point in the detector with coordinates $\overrightarrow{r}$:

$$v_1^{Det}(\overrightarrow{r}) = \frac{1}{N_{PM}} \sum_{i}^{N_{PM}} s_i \cdot f(\overrightarrow{r_i}) \cdot v_{1_i}\,. \tag{11}$$

Using (11) from (8) and (9) one can obtain the resolution at an arbitrary detector point:

$$R(Q, \overrightarrow{r}) \equiv \sqrt{\frac{\sigma_Q^2(\overrightarrow{r})}{Q^2(\overrightarrow{r})}} = \sqrt{\frac{1 + \frac{1}{f_s(\overrightarrow{r})} v_1^{Det}(\overrightarrow{r})}{f_s(\overrightarrow{r}) \cdot Q_0}}. \tag{12}$$

If the number of PMTs is big enough, then the mean value of the product in the definition of the parameter $v_1^{Det}(\overrightarrow{r})$ can be substituted by the product of the mean values:

$$v_1^{Det}(\overrightarrow{r}) \approx \frac{1}{N_{PM}} \sum_i^{N_{PM}} f_s(\overrightarrow{r}) \cdot \frac{1}{N_{PM}} \sum_i^{N_{PM}} s_i \cdot v_{1_i} = f_s(\overrightarrow{r}) \cdot v_1^{Det}(0) \,. \tag{13}$$

Then the energy resolution of the detector for the point-like source at an arbitrary point is:

$$R(Q, \overrightarrow{r}) = \sqrt{\frac{1 + v_1^{Det}(0)}{f_s(\overrightarrow{r}) \cdot Q_0}}. \tag{14}$$

As it has been pointed out before, because of the detector's symmetry the geometrical factor f_s depends mainly on the distance from the source to the detector's center r. So the energy resolution in turn depends mainly on r too :

$$R(Q, \overrightarrow{r}) \approx R(Q, r) = \sqrt{\frac{1 + v_1^{Det}(0)}{f_s(r) \cdot Q_0}}. \tag{15}$$

One can see that detector's energy resolution for the case of an arbitrary source position again behaves in the same way as the energy resolution of a single PMT (1) and is defined by the parameter $v_1^{Det}(0)$ which is defined for the source at the detector's center. The main difference between the case of a source at the detector's center (5), and the case of the source at an arbitrary position, is the geometrical factor $f_s(r)$.

2.3 CTF light collection geometrical function

In this section the geometrical functions $f(\overrightarrow{r})$ and $f_s(r)$, introduced in the previous section, are estimated using the CTF data. The CTF detector is described in detail in [3]. It consists of 4.3 tones of liquid scintillator, contained in a transparent spherical inner vessel with a diameter of 105 cm, and viewed by 100 photomultipliers (PMTs) located on a spherical steel structure support. The PMTs are equipped with light concentrator cones to increase light collection efficiency. The radius of the sphere passing through the opening of the light cones is 273 cm.

The CTF programme included a set of measurements with a ^{222}Rn source. These data were used to calibrate a reconstruction algorithm and the spatial resolution of the event reconstruction. The source consisted of a ^{222}Rn spiked scintillator contained in a quartz vial, which could be inserted into the detector[6]. The β-decay of ^{214}Bi of the ^{222}Rn decay sequence followed by the α-decay of ^{214}Po with a mean lifetime of 236 μs was used to distinguish radon events.

The events of the ^{214}Po decay are named "radon events" in further discussion. The amount of light emitted in an α-decay of ^{214}Po corresponds to 862 KeV energy deposited by an electron.

2.3.1 The method of calculation.

The geometrical function $f(\overrightarrow{r})$ has been obtained using the data with the radon source in different positions inside the inner vessel. Every source position gives N_{PMT} points for the $f(\overrightarrow{r})$ function, because every PMT "sees" the source in its own coordinate system. So even the restricted data set (50 source positions have been used) allows one to follow the geometrical function over all the range of r and Θ. For the estimations, the range of r and Θ was divided into 21x40 bins, that correspond roughly to the 5x15x15 cm^3 bins in the outer detector's region. The table $\{r_i, \Theta_i, f(r_i, \Theta_i)\}$ has been filled for every source position. After filling, the mean value at every bin has been estimated using the number of events as statistical weights. The empty bins were filled with the mean values of the non-empty neighboring bins using the same weights.

The light propagation has been extensively studied in the CTF (see [4]). The parameters obtained have been used for improvement of the Monte-Carlo simulations. In figures 2 and 3 the geometrical functions, obtained from the data and with a Monte Carlo simulation, are presented. One can see good agreement between the two functions. Two further plots (fig.4 and fig.5) present the difference between the CTF geometrical function and the solid angle only dependence. One can see significant deviations from the simple solid angle dependence for large distances of the source from the center, $r > 80$ cm (fig.5).

2.3.2 CTF geometrical factor $f_s(r)$

The dependence of the $f_s(r)$ factor on the source distance from the detector's center is plotted in fig.6. The volume of the detector has been divided into 10x10x10 cm^3 bins. The value of the f_s function was calculated for each bin, as shown by dots in scatter plot 6. The nominal source positions are shown on the same plot as well (stars). One can see significant fluctuations of the detector's f_s function for source positions with $r > 60$ cm. This is the result of the nonuniformity of the distribution of the working PMTs during the last CTF runs. For the considered run only 50 PMTs were operating.

One can see also that the source positions have been chosen in the regions where the f_s function has lower values. Note that the geometrical factor is equal to 1 near the detector's center.

In order to verify the influence of the f_s factor on the CTF detector energy resolution, an analysis of the data with radon dissolved in the CTF inner vessel has been performed. During the initial stage of the CTF operation, a certain amount of radon was observed in the detector's scintillator [3]. These data have been used for the estimations. The results are presented in table 1. One can see the dependence of the energy resolution on the source position. The calculation of the $v(p)$ factor using the data from table 1 [1] (see section 2.5.1) gives the value 0.012. This value is much better than the one calculated from the data with the artificial radon source at different positions inside the CTF (this

[1] The radon data in the detector's region $r < 40$ cm were used to obtain the resolution at the detector's center $R_0^2 = \frac{18.1}{243.8}$. The radon data distributed over all the detector volume (without any spatial cuts) were used to obtain the resolution for the distributed source $R_{vol}^2 = \frac{20.9}{239.1}$. The parameter $v(p)$ can now be estimated from the simple relation $R_{vol}^2 = R_0^2 + v(p)$.

Figure 2: The CTF-I geometrical function plotted in (r,Θ) coordinates. The upper plot is the result of a MC simulation, the lower one is obtained using CTF-I data with the radon source in different positions. One can see good agreement between the experimental and the Monte-Carlo data.

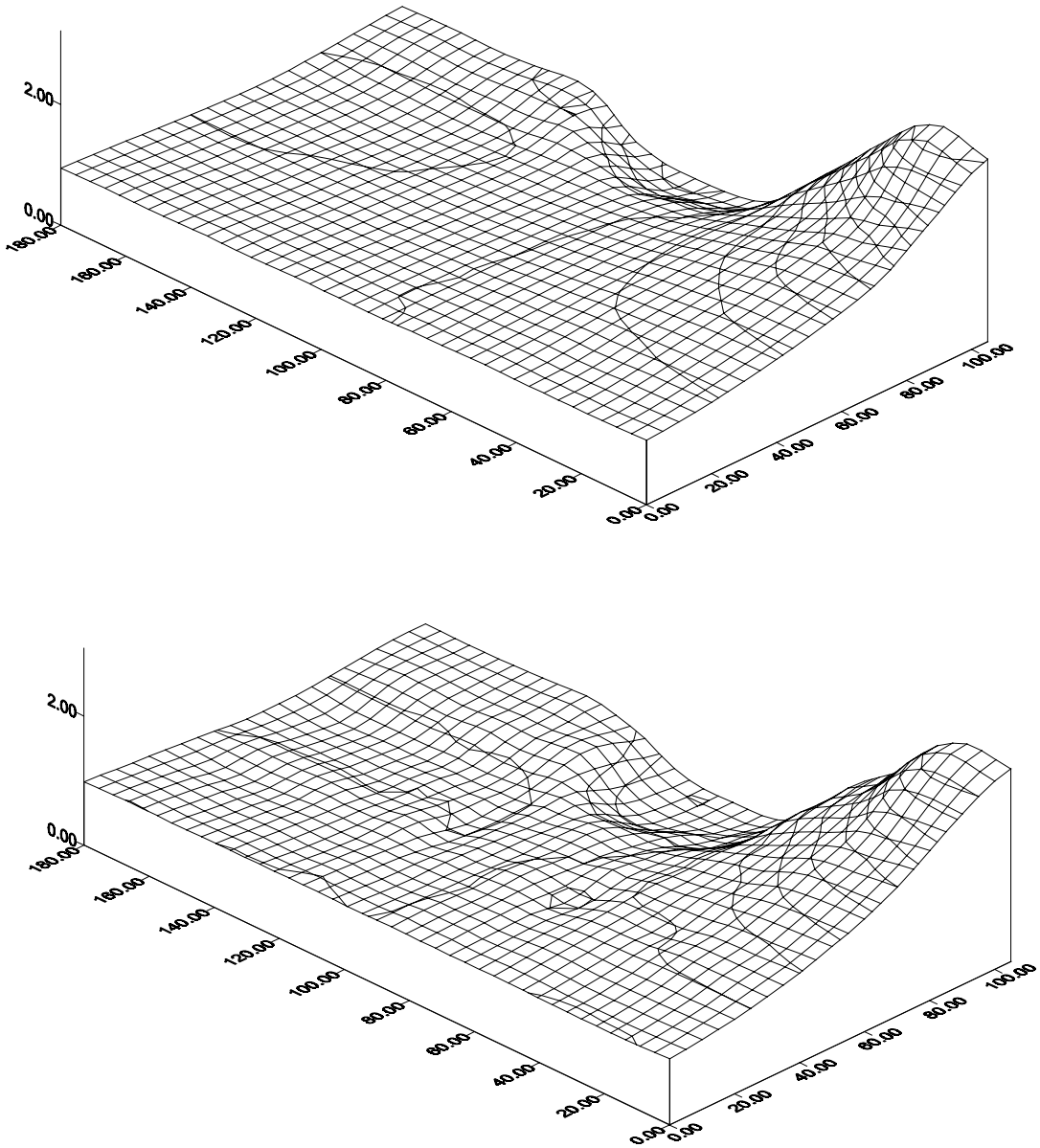

Figure 3: Isolevels for the two functions presented on the previous plot.

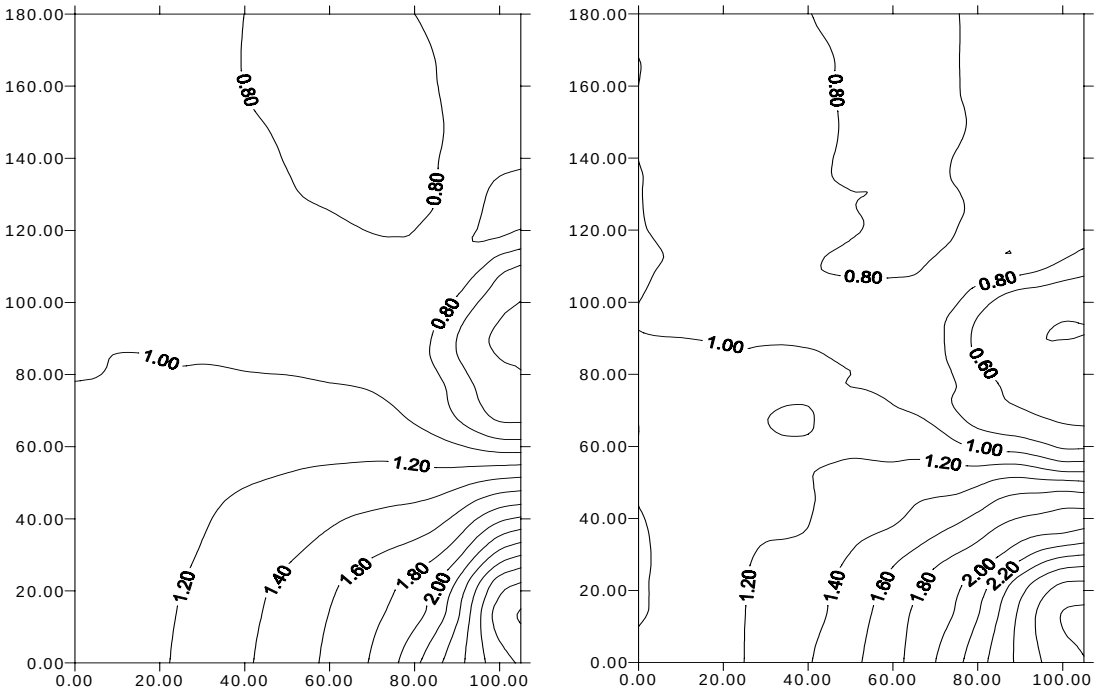

Figure 4: The difference between the CTF-I geometrical function and the solid angle dependence plotted in (r,Θ) coordinates. The upper plot is the result of a MC simulation with the solid angle dependence (presented on the lower plot) subtracted.

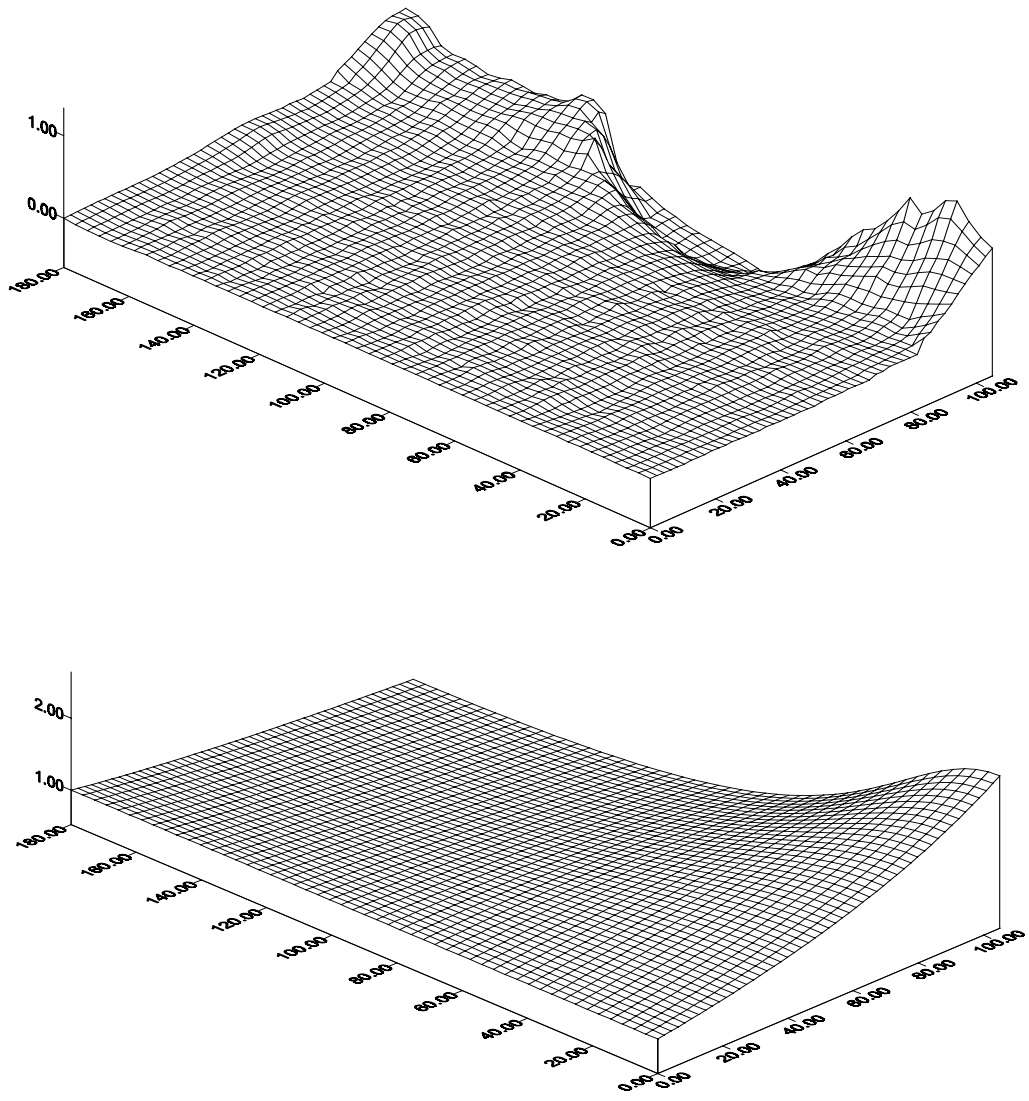

Figure 5: The difference between the CTF-I geometrical function and the solid angle dependence is visualized on this plot. Uniform color corresponds to a zero difference between the two functions. The dark region around ($r \to 105, \Theta \simeq 90^\circ$) corresponds to the "blind" region which is formed by the total internal reflection of the light at the PC-water boundary. Two other regions, that are noticeably different from the pure solid angle function, are the regions with a Θ corresponding to the closest and more distant region from the given PMT (close to the inner vessel surface).

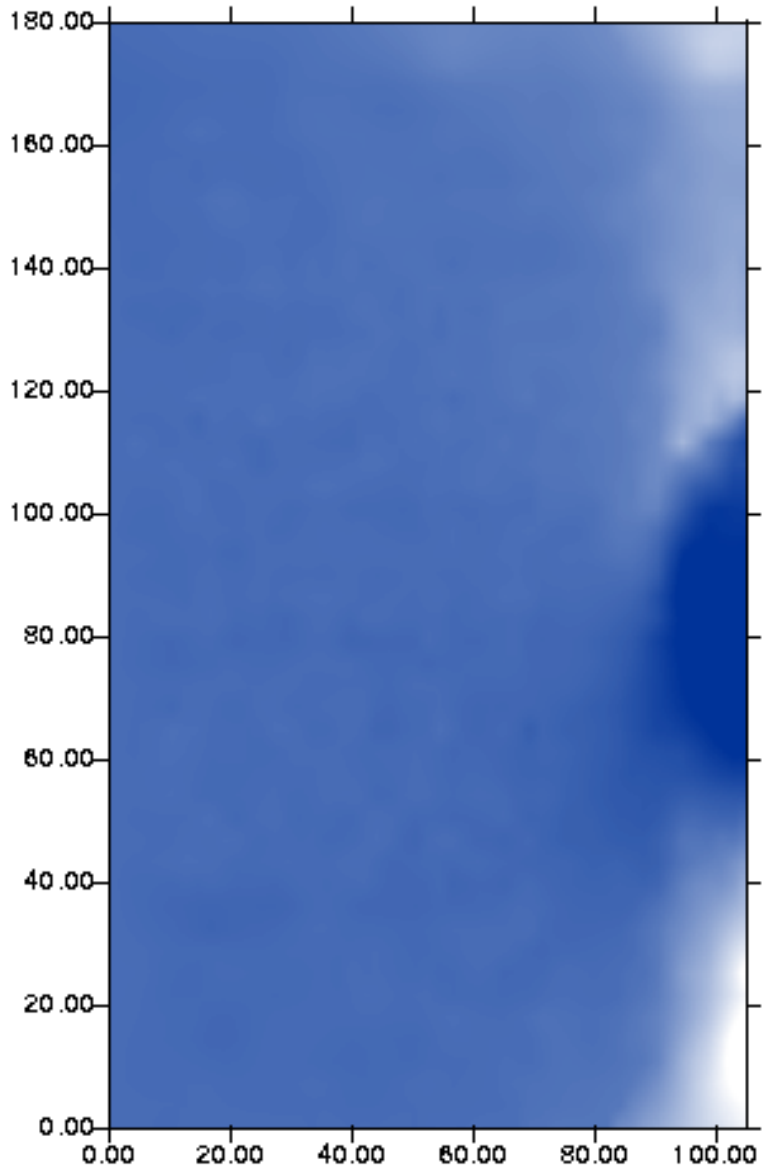

Figure 6: The dependence of the f_s factor on the source distance from the detector's center.

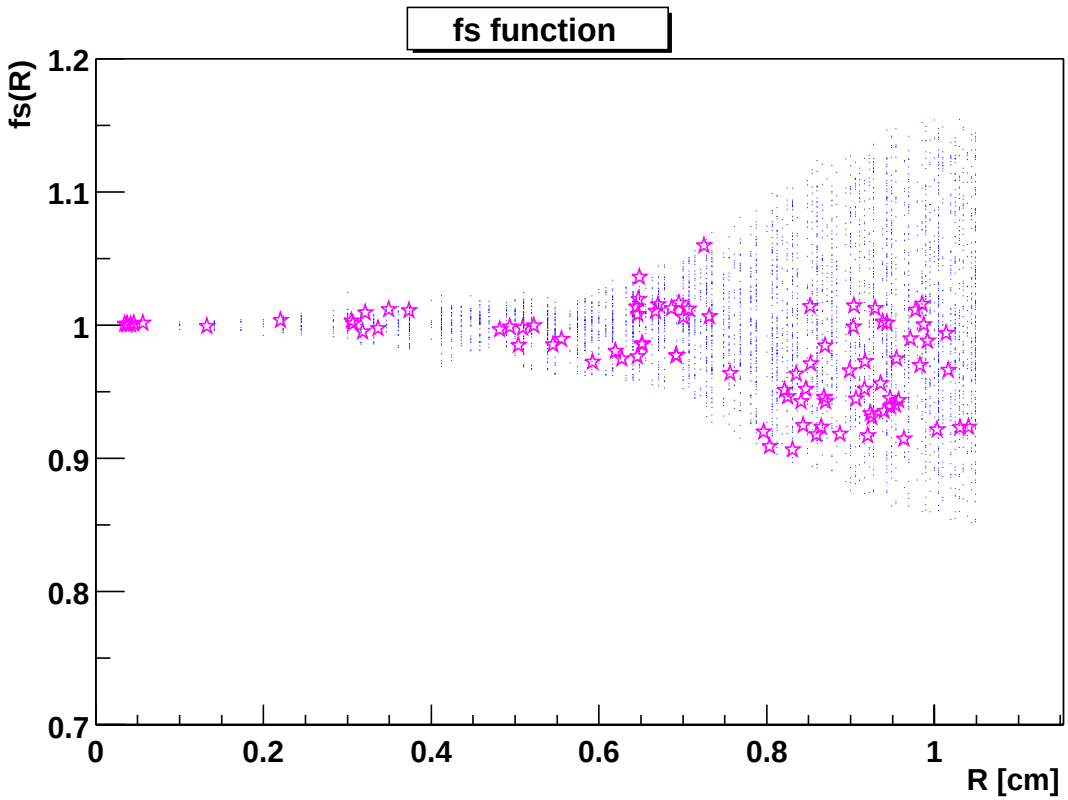

Table 1: Energy resolution for the radon dissolved in the scintillator volume.

	Data		Gauss fit		
r[cm]	$< Q >$	σ_Q	$< Q >$	σ_Q	N_{event}
$0 < r < 15$	242.2	16.5	—	—	29
$15 < r < 25$	245.6	18.5	—	—	96
$25 < r < 35$	243.8	18.4	—	—	219
$35 < r < 45$	244.5	18.0	244.0	18.0	429
$45 < r < 55$	245.6	19.4	246.2	18.7	568
$55 < r < 65$	244.1	19.0	244.8	18.4	657
$65 < r < 75$	242.7	19.5	242.5	19.3	1032
$75 < r < 85$	239.2	21.4	238.6	21.3	1132
$85 < r < 95$	235.5	21.3	235.9	21.5	1172
$95 < r < 105$	231.3	21.2	231.0	21.2	762
$0 < r < 40$	243.9	18.1	243.8	17.7	529
$0 < r < 50$	244.6	18.6	244.6	18.2	1831
$0 < r < \infty$	239.3	20.9	239.1	21.1	6780

value is 0.05, see section 2.3.5). The explanation is that the number of working PMTs in these runs is different. During the measurements with the artificial radon source, only about 50 PMTs were operational, while in the first runs the number of PMTs was 84.

2.3.3 The dependence of the total collected charge from the source position in CTF

The total charge, registered for the different source positions is presented in fig.7 (marked by crosses). The total charge is defined as a sum of the all PMT signals. The mean value and its variance over all source positions is:

$$107.9 \pm 5.8\,(5.4\%).$$

On the same plot are shown the values of the total charge for the same source positions corrected with the f_s factor (10). The mean value and its variance over all source positions is:

$$111.0 \pm 4.4\,(3.9\%).$$

One can see that the correction with the f_s factor improves the estimation of the energy.

2.3.4 The results of the source energy reconstruction in CTF

The results of the source energy reconstruction, with a method discussed later in section 5, are presented in fig.8. The mean value and its variance for the reconstructed energy over different source position is:

Figure 7: The total charge registered for the different source positions in CTF (crosses). The values of the total charge for the same source positions corrected with the f_s function are marked with stars.

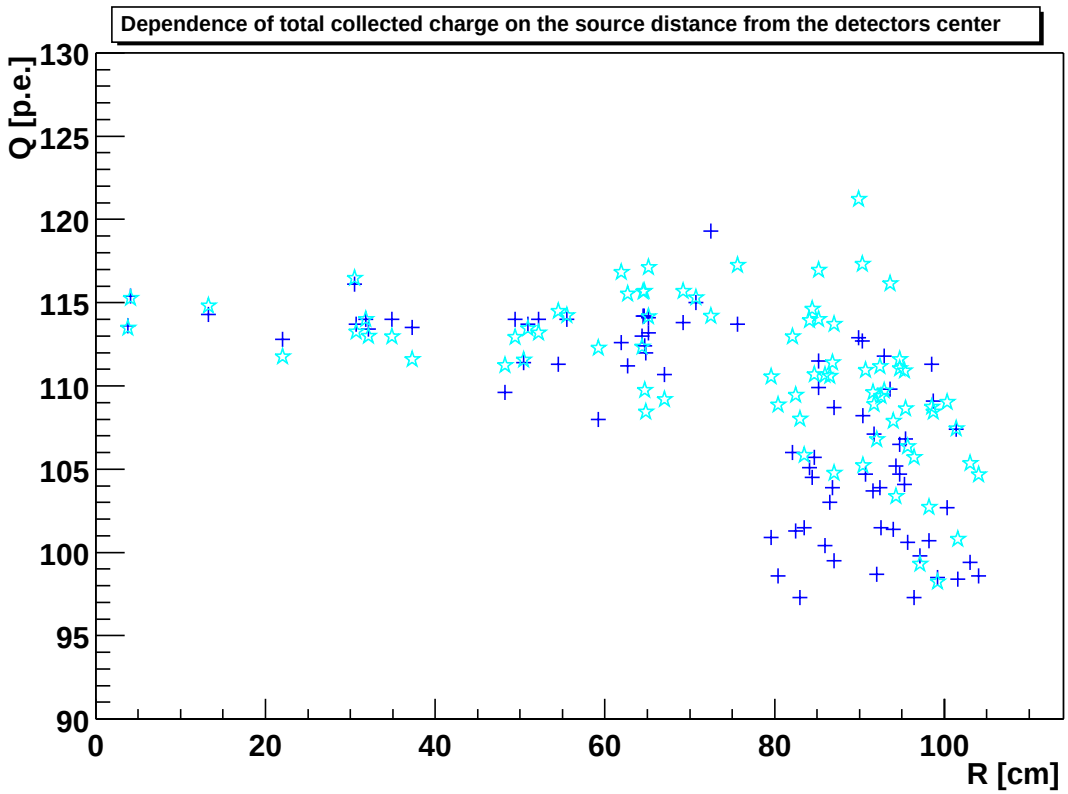

$$137.9 \pm 3.9\,(2.8\%).$$

One can notice a big difference between the mean values obtained by summing PMT signals (107.9) corrected with the f_s factor (114.4), and the value obtained with a combined position and energy reconstruction (137.9). The origin of this difference is the method used for the SER calibration. In the standard CTF reconstruction program the position of the SER is taken as the calibration value (i.e. the charge corresponding to 1 p.e.). The reconstruction with PMT charge signals needs a more precise calibration of the PMTs using the mean value of the SER. This is discussed in detail in [5]. For a typical PMT the position of the mean is $15 - 20\%$ lower that the position of the peak (or the most probable value). This difference has no influence on the detector energy resolution (see section 2.4 for the explanation). The only noticeable change is the energy scale factor (used to transform p.e. to energy).

2.3.5 Some integrals of the CTF geometrical functions

Some integrals were calculated for the geometrical function obtained from the CTF data. The mean value of the f_s function over the detector volume is $< f_s(r) >_V = < f(r) >_V = 1.00$. This value means there is a very high detectors uniformity with respect to the total collected charge.

The relative variance of the CTF geometrical factor turns out to be $v(f_s) = 0.05$. It is easy to check that the influence of the $v(p)$ factor on the detector's resolution will be noticeable at energies above 70 KeV (estimated from the equation $\frac{1+v_1}{Q} = v(p) = 0.05$). So, even at the ^{14}C energies, the deviation from the $\frac{const}{\sqrt{Q}}$ law will be noticeable.

For comparison, the mean quadratic value of the single PMT geometrical function is: $< f^2(r) >_V = 1.16$. So, the variance of the geometrical function for the single PMT is much higher than for the whole detector $v(f(r)) = 0.16$. This should be taken into account when estimating the PMT parameters using the events distributed over the detector's volume.

2.4 Influence of the calibration precision on the detector energy resolution

The calibration of the PMT means establishing the scale for the PMT anode charge in registered photoelectrons. Assuming the linearity of the registration process, one can describe the accuracy of the PMT calibration with just one parameter:

$$c_i = \frac{\mu_i'}{\mu_i}, \tag{16}$$

where μ_i' is the i-th PMT charge (or p.e. number) defined applying the calibration, and μ_i is the real charge.

Figure 8: The result of the combined reconstruction (using time and charge data) are shown with circles. The total charge registered for the different source positions, defined as a sum over all PMTs, is shown for comparison (marked by crosses). The reconstruction results are renormalized in order to make the comparison more evident (the point at $r \sim 0$ cm has been used for renormalization).

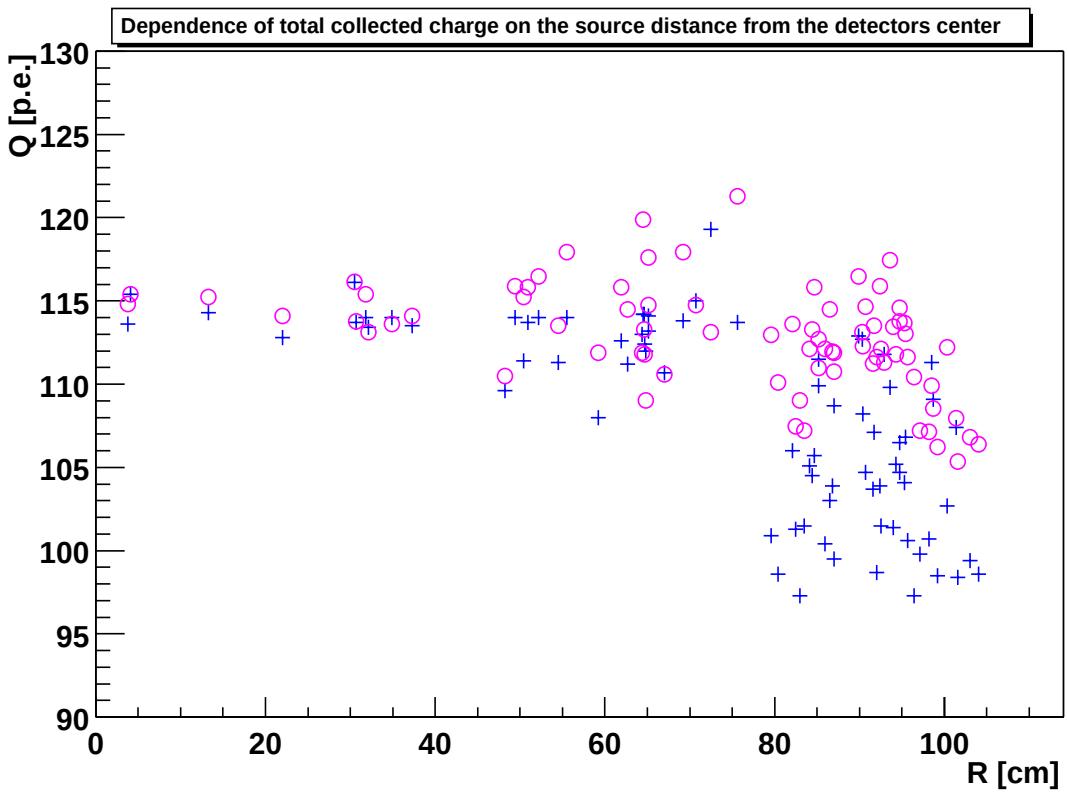

The relative variance of the registered charge for each PMT doesn't depend on a calibration used, and is defined by the relative variance of the PMT single photoelectron response v_1 as:

$$\left(\frac{\sigma_{\mu'}}{\mu'}\right)^2 = \left(\frac{\sigma_\mu}{\mu}\right)^2 = \frac{1+v_1}{\mu}. \tag{17}$$

The detector signal (full charge for an event) is defined summing the charge on the individual PMTs:

$$Q\prime = \sum_i^{N_{PM}} \mu\prime_i = Q \cdot \frac{1}{N_{PM}} \sum_i^{N_{PM}} c_i s_i \tag{18}$$

Here s_i is the relative sensitivity of the i-th PMT defined as $s_i = \frac{\mu_i}{\mu_0}$, where $\mu_0 = \frac{Q}{N_{PM}}$ is the mean charge registered by one PMT in an event.

From the point of view of probability theory the detector signal is a convolution of the signals on the individual PMTs. Hence the detector signal variance can be calculated by summing variances from the PMTs:

$$\sigma^2_{Q\prime} = \sum_i^{N_{PM}} \sigma\prime^2_{\mu_i} = \sum_i^{N_{PM}} \frac{(\mu\prime_i)^2}{\mu_i}(1+v_{1_i}) = \sum_i^{N_{PM}} c_i^2 \mu_i (1+v_{1_i}) =$$

$$\mu_0 \sum_i^{N_{PM}} c_i^2 s_i + \mu_0 \sum_i^{N_{PM}} c_i^2 s_i v_{1_i} = Q \cdot \left(\frac{1}{N_{PM}} \sum_i^{N_{PM}} c_i^2 s_i + \frac{1}{N_{PM}} \sum_i^{N_{PM}} c_i^2 s_i v_{1_i}\right). \tag{19}$$

So the energy resolution of the detector for the considered calibration is in this case:

$$R'(Q) = \sqrt{\frac{\frac{1}{N_{PM}} \sum_i^{N_{PM}} c_i^2 s_i + \frac{1}{N_{PM}} \sum_i^{N_{PM}} c_i^2 s_i v_{1_i}}{Q \cdot (\frac{1}{N_{PM}} \sum_i^{N_{PM}} c_i s_i)^2}} = \frac{const}{\sqrt{Q}}. \tag{20}$$

In the case when the number of PMTs is big enough (in practice > 50) it is possible to replace the means of the product in (20) with the product of the means. Taking into account that $< s >= 1$ by its definition, and $< c^2 >=< c >^2 + \sigma_c^2$, the formula (20) is significantly simplified:

$$R'(E) = R(E)\sqrt{1+v(c)}, \tag{21}$$

where $v(c) \equiv \left(\frac{\sigma_c}{\bar{c}}\right)^2$ is the relative variance of the calibration "nonaccuracy".

One can see that the detector energy resolution is quite insensitive to the individual PMT's calibration. Indeed, the moderate precision of the PMT calibration of 20% (i.e. $\sigma_c = 0.2$) will cause only 2% ($\sqrt{1+0.2^2}$) worsening of the detector's resolution.

2.5 The energy resolution for a non point-like source

2.5.1 A monoenergetic source

For a point-like source with an energy E at a position $\overrightarrow{r}$, the i-th PMT will register a mean number of photoelectrons:

$$\mu_i(\overrightarrow{r_i}, E) = f(\overrightarrow{r_i}) \cdot \mu_0(E) \cdot s_i \,.$$

Here the independence of the geometrical function from the source energy is assumed:

$$f(\overrightarrow{r}) \equiv \frac{\mu(\overrightarrow{r})}{\mu(\overrightarrow{0})} \tag{22}$$

and s_i is the relative sensitivity of the i-th PMT.

The total registered charge (summed over all PMTs) is:

$$Q(r, E) = \sum_{i=1}^{N_{PM}} f(\overrightarrow{r_i}) \cdot \mu_0 \cdot E \cdot s_i = \mu_0 \, E \cdot N_{PM} \cdot \frac{1}{N_{PM}} \sum_{i=1}^{N_{PM}} f(\overrightarrow{r_i}) \, s_i \,.$$

The mean value of the relative sensitivity is equal to 1 by the definition: $< s >= \frac{1}{N_{PM}} \sum_{i=1}^{N_{PM}} s_i = 1$. Using the definition of $f_s\,(r)$ one can write:

$$Q(r, E) = Q_0(E) \cdot f_s\,(r) \,.$$

If a source with an energy E is uniformly distributed over the detector's volume with density $n(r)$, then the mean registered charge is:

$$< Q >= Q_0(E) \cdot \int_0^{R_0} f_s\,(r)\, n(r)\, dr \equiv Q_0(E) < f_s > \,. \tag{23}$$

The mean value of the detector's function $< f_s >_R$ is equal to the mean value of the single PMT function $< f >_V$.

For a point-like source the distribution of registered charge is the convolution of the charge distributions for the individual PMTs, hence the variation of the registered charge is the sum of the individual variations:

$$\sigma^2(r, E) = \sum_{i=1}^{N_{PM}} \sigma_i^2\,(r_i, E) = \sum_{i=1}^{N_{PM}} \mu_i\,(r_i, E)\,(1 + v_{1_i}) = Q_0(E)\, f_s(r)\,(1 + \overline{v_1}) \,.$$

For the source uniformly distributed over the detector volume, the mean of the total charge squared can be obtained by averaging the values of the charge squared at every point in the detector:

$$< Q^2(E) >=< Q(r,E)^2 + \sigma(r,E)^2 >_V =$$

$$= Q_0^2(E) < f_s^2(r) >_V + Q_0(E)(1+\overline{v_1}) < f_s(r) >_V =$$

$$= Q_0^2(E) < f_s^2(r) >_V + Q_0(E)(1+\overline{v_1}) < f_s > . \quad (24)$$

The variation of the total charge is then:

$$\sigma_Q^2(E) =< Q^2 > - < Q >^2 = Q_0^2(E)(< f_s^2(r) >_V - < f_s >^2) + Q_0(E)(1+\overline{v_1}) < f_s > .$$

And, finally, the resolution

$$R_V(E) = \sqrt{\frac{\sigma_Q^2(E)}{Q^2(E)}} = \sqrt{\frac{1+\overline{v_1}}{Q_0(E) < f_s >} + v(f_s)} . \quad (25)$$

Here $v(f_s)$ is the relative variance of the $f_s(r)$ function over the detector volume:

$$v(f_s) \equiv \frac{< f_s^2(r) >}{< f_s >^2} - 1.$$

It should be pointed out that $v(f_s)$ has the same sense as $v(p)$ in formula (2).

2.5.2 A source with energy spectrum $f_E(E)$

If a source is uniformly distributed over the detector's volume with density $n(r)$, and its energy spectrum is described with a function $f_E(E)$ then the mean charge registered by the detector is:

$$< Q >= Q_0 \cdot \int_{E>E_{th}} E\, f_E(E)\, dE \cdot \int_0^{R_0} f_s(r)\, n(r)\, dr \equiv Q_0 < E >< f_s > . \quad (26)$$

The proportionality of the registered charge Q and the source energy E is assumed here. Thus, $Q(E) = Q_0 \cdot E$, where Q_0 is a proportionality coefficient (i.e. the charge registered for the unit energy deposition).

For the source uniformly distributed over the detector's volume with an energy spectrum $f_E(E)$ the mean value of the registered charge squared can be obtained by averaging the mean quadratic values of the charge registered over the detector's volume:

$$< Q^2 >=< Q(r,E)^2 + \sigma(r,E)^2 >_{V,E} = Q_0^2 < E^2 f_s^2(r) >_{V,E} + Q_0(1+\overline{v_1}) < E f_s(r) >_{V,E} =$$

$$= Q_0^2 < E^2 >< f_s^2(r) >_V + Q_0(1+\overline{v_1}) < E >< f_s > . \quad (27)$$

So that the variation of the total registered charge is (using (26) and (27)):

$$\sigma_Q^2 =< Q^2 > - < Q >^2 = Q_0^2(< E^2 >< f_s^2(r) >_V - < E >^2 < f_s >^2) + Q_0(1+\overline{v_1}) < E >< f_s > .$$

and the relative variance of the detector response is:

$$Var_{V,E}(Q) \equiv \frac{\sigma_Q^2}{< Q >^2} = \frac{1+\overline{v_1}}{Q_0 E < f_s >} + v(f_s) + v(E) + v(f_s)v(E), \quad (28)$$

where $v(E)$ is the relative variance of the source energy spectrum

$$v(E) \equiv \frac{< E^2 > - < E >^2}{< E >^2}.$$

3 Reconstruction using charge signals

The reconstruction of an event position and energy is performed using the maximum likelihood method with 4 free parameters: 3 coordinates of the event and the event energy. The likelihood function has the following form:

$$L(x,y,z,Q_0) = log\left(\prod_{i=1}^{N_{PM}} p\left(\mu(\overrightarrow{r_i}(x,y,z),Q_0),q_i\right)\right), \quad (29)$$

where $p\left(\mu(\overrightarrow{r_i}(x,y,z),Q_0),q_i\right)$ is the probability to register charge q_i at the i-th PMT for the event at a position with coordinates $\overrightarrow{r} = \{x,y,z\}$ and the total charge Q_0 (this total charge corresponds to an event of the same energy at the detector's center). Here $\overrightarrow{r}_i(x,y,z)$ are the coordinates of the event in the i-th PMT coordinate system. Using the geometrical function $f(\overrightarrow{r})$ and the relative sensitivities s_i one can write:

$$\mu(\overrightarrow{r_i},Q) = f(\overrightarrow{r_i}) \cdot s_i \cdot \frac{Q}{N_{PM}}. \quad (30)$$

The probability to register charge q at the i-th PMT if the mean expected charge is μ can be written as:

$$p\left(\mu,q\right) = \sum_{N=0}^{N_{Max}} P(N,\mu) f_N(q)\,. \quad (31)$$

This function is discussed in detail in our article [5]. For simplicity the average parameters have been used, i.e. all PMTs were described using the same set of parameters.

In the reconstruction, the initial Q_0 value used is the sum over all PMTs.

The relative sensitivities of the PMTs for the group II electronics (see [3] for the CTF electronics description) were defined using the data with the artificial radon source at the detector's center. The relative sensitivities of the PMTs for the group I electronics were defined using the ^{14}C data (because of the detector's spherical symmetry the amount of light collected by each PMT for such events should be the same).

The algorithm of the likelihood function construction can be divided into the following steps:

1. The initial total charge value Q_0 is defined as the sum of the charge registered at the individual PMTs.

2. The initial coordinates (x, y, z) of the event are guessed on the basis of the signal distribution symmetries.

3. At this point a cycle starts over all PMTs. First of all, the mean charge $\mu(\overrightarrow{r_i}, Q)$ expected at the i-th PMT is defined using formula (30);

4. Then the probability p_i to register charge q_i at the i-th PMT for the event at a position with coordinates $\overrightarrow{r} = \{x, y, z\}$ is calculated using formula (31);

5. Then the value of the likelihood function is increased by the $log(p_i)$, and the algorithm is repeated starting from point 3.

In figures 9,10 and 11 are shown examples of reconstruction using the charge signals, compared to the reconstruction using the time signals, for the different source positions (CTF data with the artificial radon source are used). One can see that the reconstruction using the time signals is better for small r (source close to the detector's center), while the reconstruction with the charge signals at $r \geq 60$ cm is comparable to the reconstruction with the time signals. The reconstruction with the charge signals for the source close to the inner vessel is better than the reconstruction with the time signals.

3.1 Analysis of the precision of the spatial reconstruction using the charge data

Let us consider an event of an energy E at a position $r = \{x, 0, 0\}$. Because of the detector's spherical symmetry this case is quite common. It is easy to recalculate the source position for every PMT in it's own coordinate system.

When the source is moved by Δx the mean registered charge will change by

$$\Delta\mu = \mu_0 \, s_i \, \frac{df(r, \Theta_i)}{dx}(x, 0, 0)\Delta x \, .$$

Figure 9: Examples of the reconstruction with the source close to the center. The reconstructed X,Y and Z coordinates are shown.

r=0 cm (red lines-reconstruction with charge signals, black one- reconstruction with time signals)

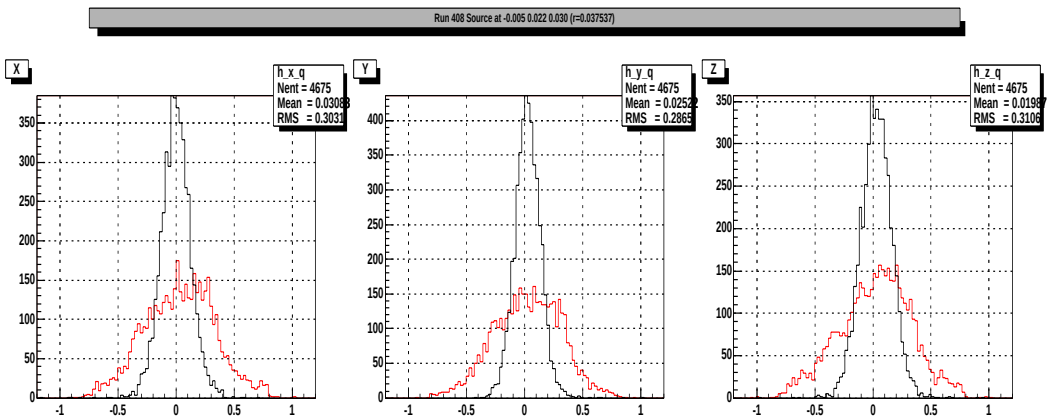

r=40 cm

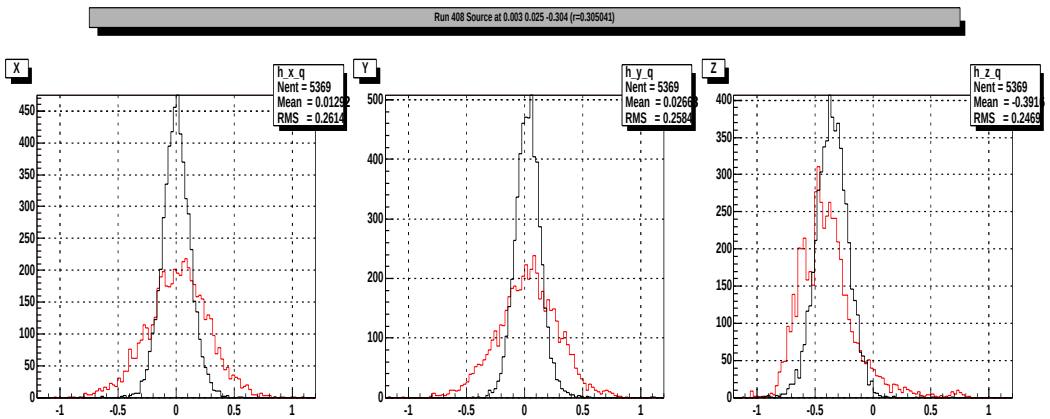

Figure 10: Examples of the reconstruction with the source far away from the center. The reconstructed X,Y and Z coordinates are shown.
r=65 cm (red dashed lines-reconstruction with charge signals, black solid one-reconstruction with time signals)

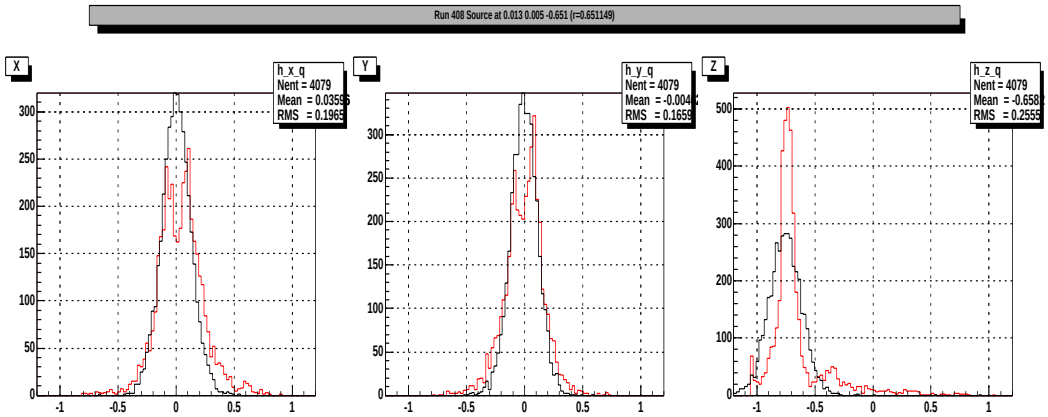

r=83 cm

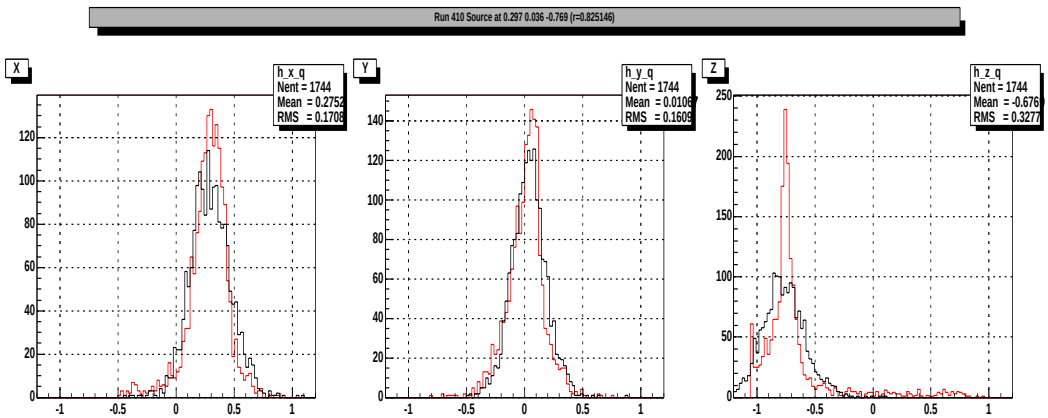

Figure 11: Examples of the reconstruction with the source at different positions inside the detector's volume. The distance between the nominal source position and the reconstructed one is shown.

r(0,0,0)=0 cm & r(0,0,-40)=40 cm

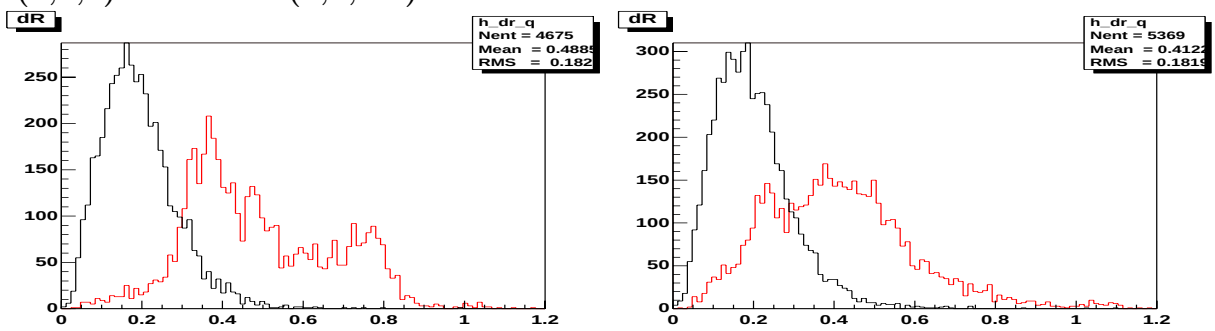

r(0,0,-80)=80 cm & r(30,4,-77)=83 cm

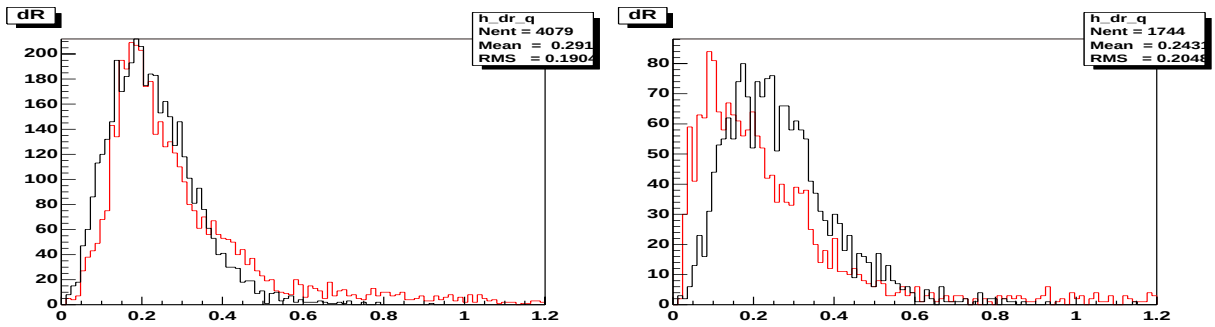

r(25,23,86)=93 cm & r(32,0,105)=105 cm

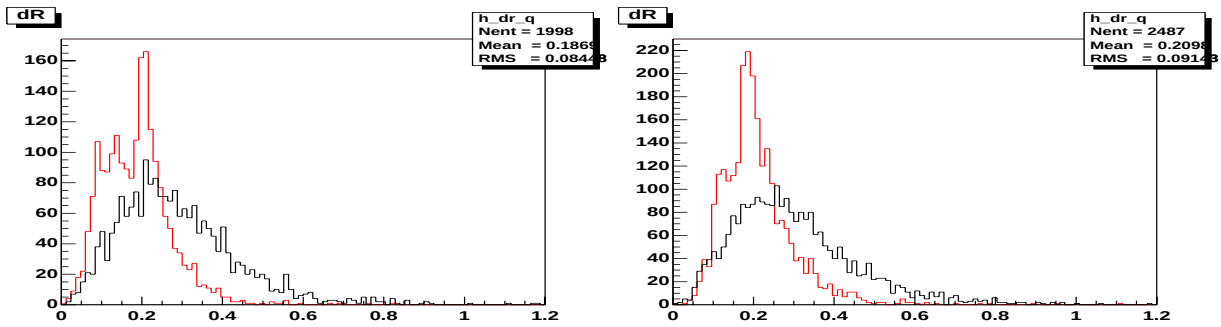

Figure 12:

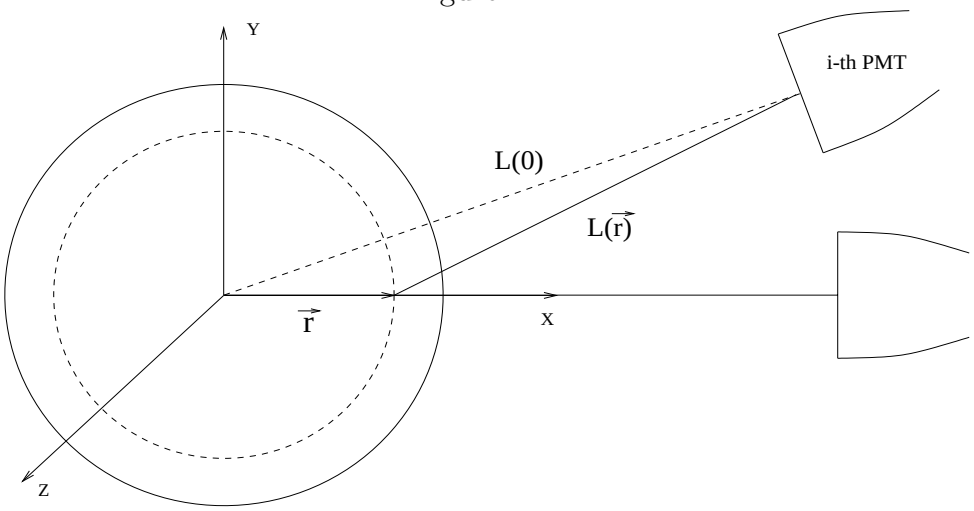

Replacing $\Delta\mu$ by the uncertainty of the charge registered $\sigma_\mu^2 = \mu_0\, s_i\, f(\overrightarrow{r})(1+v_{1_i})$ and adding quadratically the error of the registered charge reconstruction

$$\sigma_q^2 = \frac{\sigma_Q^2}{N_{PM}} = \frac{1}{N_{PM}} \frac{1+v_1^{Det}}{f_s(r) Q_0} \cdot (f_s(r)\, Q_0)^2 = \mu_0 (1+v_1^{Det})\, f_s(r)$$

(if the source energy is unknown a priori) one can write for a single PMT:

$$\sigma_{x_i} = \sqrt{f(\overrightarrow{r_i}) \frac{1+v_{1_i}}{\mu_0} + \frac{f_s(r)}{s_i} \frac{1+v_1^{Det}}{\mu_0}} \cdot \Big(\frac{df(r)}{dx}(r_i)\Big)^{-1}. \tag{32}$$

The signals on the PMTs are independent, so for the whole detector:

$$\sigma_x \geq \frac{1}{\sqrt{\sum \frac{1}{\sigma_{x_i}^2}}} = \frac{1}{\sqrt{\sum \frac{1}{f(\overrightarrow{r_i}) \frac{1+v_1}{\mu_0} + \frac{f_s(r)}{s_i} \frac{1+v_1^{Det}}{\mu_0}} \big(\frac{df(r)}{dx}(r_i)\big)^2}} =$$

$$= \frac{1}{\sqrt{\frac{\mu_0 N_{PM}}{1+v_1^{Det}} \frac{1}{N_{PM}} \big(\frac{s_i}{s_i\, f(\overrightarrow{r_i}) \frac{1+v_{1_i}}{1+v_1^{Det}} + f_s(r)}\big) \big(\frac{df(r)}{dx}(r_i)\big)^2}} =$$

$$= \frac{R_0(E)}{\sqrt{\frac{1}{N_{PM}} \big(\frac{s_i}{s_i\, f(\overrightarrow{r_i}) \frac{1+v_{1_i}}{1+v_1^{Det}} + f_s(r)}\big) \big(\frac{df(r)}{dx}(r_i)\big)^2}}. \tag{33}$$

It is convenient to change to the PMT coordinate system and to replace the summing with integration:

$$\sigma_r(r) \geq R_0(E) \Big(\frac{1}{2} \int_0^\pi \frac{1}{f(r,\Theta) + f_s(r)} \big(\frac{df(r,\Theta)}{dr}\big)^2 sin(\theta) d\theta\Big)^{-\frac{1}{2}}. \tag{34}$$

Here the differentiation over x in the detector's coordinate system is replaced by differentiation over r in the PMT coordinate system. In fact $\sigma_r(r)$ is the detector's radial resolution. The azimuthal resolution can be obtained in the same way (the factor 1/2 comes from the averaging over ϕ angle):

$$\sigma_\Theta(r) \geq R_0(E)\Big(\frac{1}{2}\cdot\frac{1}{2}\int_0^\pi \frac{1}{f(r,\Theta)+f_s(r)}\Big(\frac{df(r,\Theta)}{r\sin(\Theta)d\Theta}\Big)^2\sin(\Theta)d\Theta\Big)^{-\frac{1}{2}}. \tag{35}$$

Because of the detector's spherical symmetry the radial and the azimuthal resolutions define the total detector's resolution at any point in the detector.

3.1.1 Simple geometrical function

For estimation of the detector's resolutions let us use a simplified geometrical function of the detector (preserving only solid angle dependence)

$$f(\vec{r}) = \frac{L^2(0)}{L^2(\overrightarrow{r})}cos(\theta)\,, \tag{36}$$

where $L(\overrightarrow{r})$ is the distance between the source and the PMT, and θ is the angle of incidence of light on the PMT. From elementary geometrical considerations (see fig.12) one can obtain:

$$L^2(\overrightarrow{r}) = r^2 + L^2(0) - 2rL(0)cos(\Theta_0)\,,$$

where θ_0 is the azimuthal angle of the PMT and $r\cdot cos(\Theta_0) + L(r)cos(\Theta) = L(0)$.

If the detector's radius is $L_0 \equiv L(0)$ then the simplified geometrical function is:

$$f(\overrightarrow{r}) = \frac{L_0^2}{L^3(\overrightarrow{r})}(L_0 - r\cdot cos(\Theta_0))\,. \tag{37}$$

The precision of the spatial reconstruction at the detector's center, calculated with the function (37), is:

$$\sigma_x^{(q)} = \sqrt{\frac{3}{2}}L_0R_0(E)\,, \tag{38}$$

where $R_0(E)$ is the energy resolution at the detector's center.

3.1.2 Simple geometrical function with absorption

A better approximation for the energy resolution at the detector's center can be obtained taking into account the light absorption in the scintillator. If, for an event with coordinates $\overrightarrow{r}$, the path of light in the scintillator is $L_1(\overrightarrow{r})$, then the simplified geometrical function will have the following form:

$$f(\overrightarrow{r}) = \frac{L_0^2}{L^3(\overrightarrow{r})}(L_0 - r\cdot cos(\Theta_0))\cdot exp(-\frac{L_1(\overrightarrow{r})}{L_A} + \frac{R_{Det}}{L_A})\,, \tag{39}$$

where R_{det} is the detector radius. The exponential factor is equal to 1 at the detector's center ($L_1(0) = R_{det}$ by definition).

The precision of the spatial reconstruction at the detector's center calculated with this function is:

$$\sigma_x^{(q)} = \sqrt{\frac{3}{2}} L_0 R_0(E) \cdot \frac{1}{1 + \frac{L_0}{2L_A}}. \tag{40}$$

In the CTF detector the influence of light refraction at the scintillator/water interface significantly changes the geometrical function for events far away from the center.

3.1.3 Comparison of the estimations and the results of the reconstruction with the CTF data.

Fig.13 presents the comparison of the reconstruction precision obtained in the different ways, discussed in previous sections. The spatial resolutions (1σ) obtained with the standard (for the CTF) likelihood function (41), that is using the time data only, for the different distances from the detector's center are plotted with triangles (the method is described in the next section 4). The spatial resolutions (1σ) obtained with the likelihood function (29), i.e. using the charge data only, are plotted with crosses on the same plot. One can see that the spatial resolution at the detector's boundary is the same for both methods.

In the same figure the estimations using simplified geometrical functions (37) and the simple geometrical function with the light absorption (39) are plotted with solid lines. One can see that the better estimation provides the function which accounts for absorption. Nevertheless, if the source position is far away from the detector's center, both functions fail to describe the spatial resolution.

The last plot in fig.13 is the estimation of the spatial resolution with the geometrical function obtained from the CTF data (stars). This time the functions (34) and (35), used for the estimations, give the results that agree with the spatial resolutions found during the reconstruction by maximizing the likelihood function (29).

3.1.4 Spatial reconstruction using charge data (predictions for Borexino).

In the Borexino detector it is intended to use, as a buffer liquid, the pseudocumene (PC) which is the main scintillator component. In this case there will be no refraction at the inner vessel boundary and one can use the simple geometrical functions (37) and (39) for the estimations. The results of the estimation for sources with two different energies are presented in fig.14. The following parameters have been used in the calculations: $v_1 = 0.6$ and light yield of 400 p.e./MeV.

Figure 13: The spatial reconstruction precision (1σ) using the time data (triangles) and the charge data (crosses) as a function of the source distance from the detector's center. The results of the calculation using the geometrical function estimated from the CTF data are plotted with stars. The two lines corresponds to the calculation using the simplified geometrical function (upper line) and the simple geometrical function with light absorption (lower line).

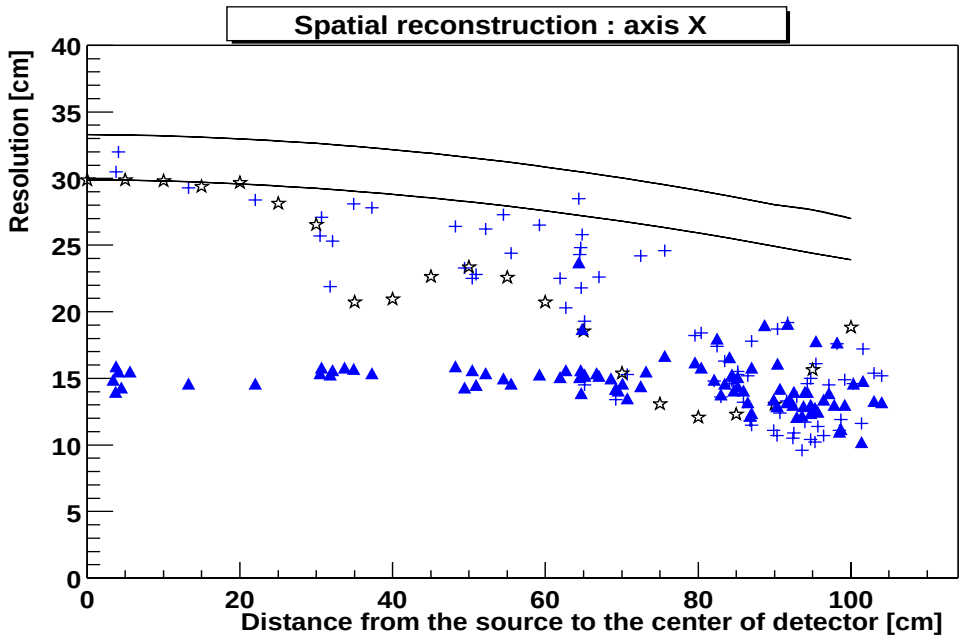

Figure 14: The precision of the spatial reconstruction for Borexino as a function of the distance from the source to the detector's center. The simple geometrical function with absorption length of 12 meters has been used in estimations.

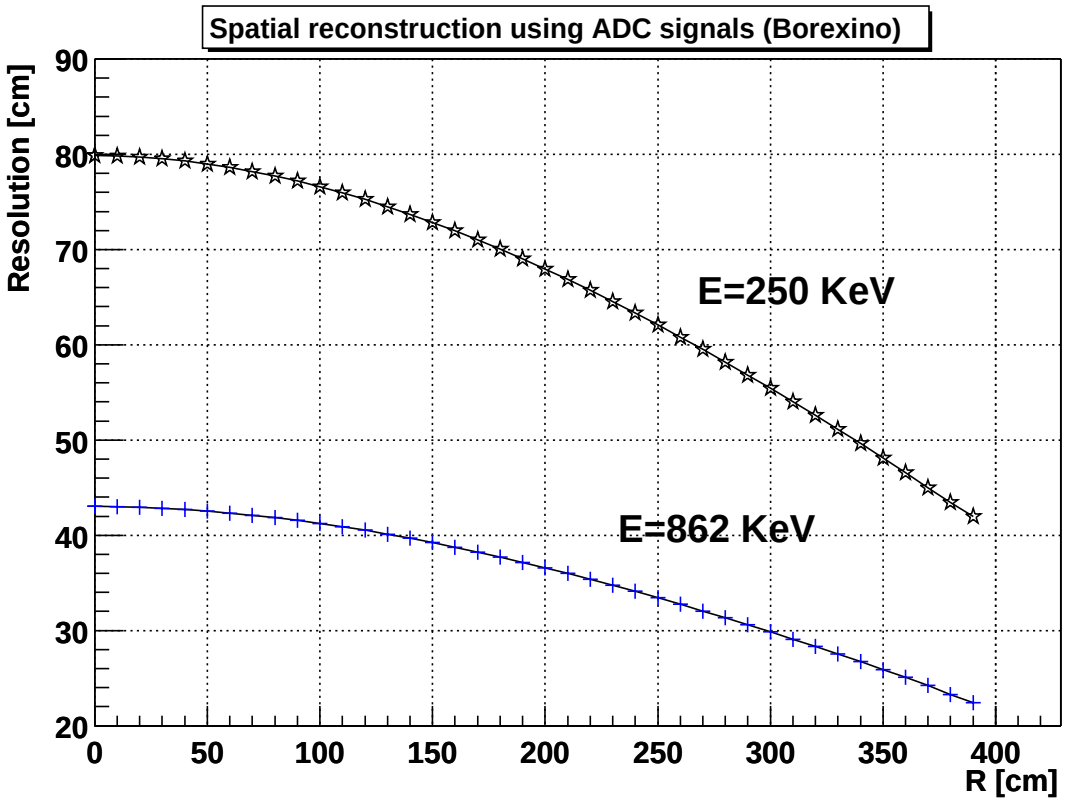

4 Reconstruction using time signals

The reconstruction of an event position is performed using the maximum likelihood method with 4 free parameters: 3 coordinates and one timing parameter τ_0, with the total charge being fixed. The likelihood function can be written as:

$$L(x,y,z,\tau_0) = log\left(\prod_{i=1,t_i<T_{max_i}}^{N_{PM}} p\left(\tau(\overrightarrow{r_i}(x,y,z),\tau_0,tdc_i),\ \mu(Q_0,\overrightarrow{r_i}(x,y,z)),\ p_t\right)\right), \quad (41)$$

where

$p\left(\tau(\overrightarrow{r_i}(x,y,z),\tau_0,tdc_i),\ \mu(Q_0,\overrightarrow{r_i}(x,y,z),\ p_t)\right)$ is the probability density function to observe the first pulse on the i-th PMT at time τ, for an event with coordinates $\{x,y,z\}$ in the detector's coordinate system, if the first photon at the i-th PMT has been registered at the time tdc_i;

$\tau\left(\overrightarrow{r_i}(x,y,z),\tau_0,tdc_i\right)$ is the function that gives the time when the first photon, registered at the i-th PMT, has been emitted. It takes into account the time of flight of the photon from the position with coordinates $\overrightarrow{r_i}(x,y,z)$ in the i-th PMT coordinates system to the i-th PMT. The parameter τ_0 coincides with $\tau\left(\overrightarrow{r_i}(x,y,z),\tau_0\right)$ for the first PMT which satisfies the relation $T_{min} < tdc_i < T_{max}$;

$\mu(Q_0,\overrightarrow{r_i}(x,y,z))$ is the mean charge registered at the i-th PMT for an event at the position with coordinates $\overrightarrow{r_i}(x,y,z)$ and the energy that corresponds to the Q_0 total charge registered for an event of the same energy at the detector's center;

Q_0 is the total charge registered for an event of the same energy at the detector's center;

τ_0 is a free parameter, its meaning will be clarified during further discussion;

p_t is the part of the SER that remains unregistered (discriminator threshold effect). It gives a renormalization factor for the p.d.f.

T_{max_i} is a hardware or software cut on the time registration at the i-th PMT (whichever cut is smaller);

$\overrightarrow{r}_i(x,y,z)$ is the event coordinate in the i-th PMT coordinate system;

(x,y,z) are the event coordinates in the detector coordinate system.

If, one of the PMTs registers an event at the time tdc_0 and the i-th PMT registers the same event at the time tdc_i, then:

$$tdc_0 = T_0 + tof_0 + tt_0 + \tau_0 \,,$$

$$tdc_i = T_0 + tof_i + tt_i + \tau_i \,,$$

where T_0 is the absolute time at which the event occurred and tof_i is the minimum time of flight for the photon from the event position $\{x, y, z\}$ to the i-th PMT. The drift time of the electrons inside the i-th PMT is tt_i, and τ_i is the moment when the first photon, registered at the i-th PMT, has been emitted. Index "0" is used for the arbitrary PMT (the first one satisfying $T_{min} < t_i < T_{max}$ condition). One can see that the time of photon registration at the i-th PMT can be calculated using the time of arrival of the photon to one of the PMTs:

$$\tau_i = \tau_0 + (tof_0 + tt_0 - tdc_0) - (tof_i + tt_i - tdc_i) \,. \tag{42}$$

Thus the time of registering of the first photon by the i-th PMT can be calculated from the time of arrival of the first photon at one of the PMTs.

The algorithm of the likelihood function construction can be divided into the following steps:

1. The initial total charge value Q is fixed to the sum of the charge registered at the individual PMTs.

2. The initial coordinates (x, y, z) of the event are guessed on the basis of the signal distribution symmetries.

3. The charge Q_0 that corresponds to the event of the same energy at the detector's center is calculated as
$$Q_0 = \frac{Q}{f_s(x, y, z)};$$

4. At this point a cycle starts over all PMTs. First of all, the condition $T_{min} < t_i < T_{max}$ is checked out. If this condition is false, the corresponding PMT is excluded from the maximum likelihood calculation.

5. The mean charge expected at the i-th PMT can be defined now as
$$\mu(\overrightarrow{r_i}, Q) = f(\overrightarrow{r_i}) \cdot s_i \cdot \frac{Q_0}{N_{PM}}; \tag{43}$$

6. For the first PMT that arrives at this point, the moment of time at which the first photon has been emitted is assumed to be τ_0, and the parameter $t_0 = tof_0 + tt_0 - tdc_0$ is calculated (see formula (42)). For all other PMTs the parameter τ_i is calculated as $\tau_i = \tau_0 + t_0 - (tof_i + tt_i - tdc_i)$;

7. Now the cut time at the i-th PMT T_{cut_i} is calculated using formula (48) of the next section;

8. Then the probability of the PMT hit at the moment τ_i is calculated: $p_i = \rho(\tau_i, \mu_i, p_t)$;

9. The conditional probability of the PMT hit at the moment τ_i is calculated as $pc_i = \frac{p_i}{F(T_{cut_i}, \mu_i, p_t)}$, where $F(T_{cut_i}, \mu_i, p_t) = \int_{T_{min}}^{T_{cut_i}} \rho(t, \mu_i, p_t)dt$ is the total probability to register a p.e in the time interval up to T_{cut_i};

10. The value of the likelihood function is increased by $log(pc_i)$ and the algorithm is repeated starting from point 4.

The p.d.f. (probability density function) of the registration time of the first photon $\rho_1(t)$ has been studied in laboratory conditions [7]. The conditions were set in such a way that a PMT was registering practically a single p.e. (the mean number of the registered p.e. were about 0.05) with p.d.f. $\rho(t) \simeq \rho_1(t)$. The time of the scintillation occurrences were measured by another PMT with a high precision. It is easy to show that the pdf of the registration time t for the light pulse with the mean p.e. number μ is

$$\rho(t) = \frac{\mu \cdot \rho_1(t)}{1 - e^{-\mu}} e^{-\mu F(t)}. \tag{44}$$

where $F(t) = \int_{-\infty}^{t} \rho_1(t)dt$. In order to take into account the transit time of the PMT $\rho_{TT}(t)$ it is necessary to replace : $\rho_1(t) \rightarrow \rho_1(t) \otimes \rho_{TT}(t)$ (the sign $\otimes$ is used for the convolution of two functions).

It is important to notice that it was assumed that the p.d.f. of the time of the registering of the first photon is independent of the source position.

4.1 Analysis of the precision of spatial reconstruction using time data

When reconstructing an event position using (41) one should note that late registered photons do not provide information about the event coordinates, so such signals should be excluded from the analysis. The influence of the different "time cuts" on the reconstruction precision is investigated below. The T_{cut} is counted from the moment $(T_0 + tof_{min})$ where T_0 is an event occurrence time, and tof_{min} is time of flight to the closest PMT in the detector.

The uncertainty of the time of arrival of the photon to a single PMT is:

$$\sigma_t(T) = \frac{\sqrt{\sigma^2(T) + \sigma^2_{T_0}(T)}}{1 - e^{-\mu F(T)}}, \tag{45}$$

where

$$\sigma^2(T) = \frac{\int_{-\infty}^{T}(t - \overline{t(T)})^2 \rho(T) dt}{F(T)}, \tag{46}$$

and

$$\sigma^2_{T_o} = [\sum_{i}^{N_{PM}} \frac{1 - e^{-\mu F(T_i)}}{\sigma^2_i(T)}]^{-1} \tag{47}$$

is the uncertainty of the reconstruction of T_0 for an event with known coordinates. The denominator $1 - e^{-\mu F(t)}$ reflects the fact that the photon is registered in the time interval $[-\infty, T]$). The "cut time" for the i-th PMT is:

$$T_{cut_i} = T_{cut} + T_0 + tof_{min} - tof_i \, . \tag{48}$$

So, the closer to a PMT the event occurs, the bigger is the "cut time".

Using simple geometrical relations one can write:

$$L(r, \Theta) = \sqrt{L_0^2 + r^2 - 2 \cdot r \cdot L_0 \cdot \cos(\Theta)} \, ,$$

so

$$\frac{dL}{dr} = \frac{r - L_0 \cdot \cos(\Theta)}{L(r, \Theta)}$$

and

$$\frac{dL}{d(\cos(\Theta))} = -\frac{r \cdot L_0 \cdot \cos(\Theta)}{L(r, \Theta)}.$$

A small change of the source position by Δr along the radius can be registered by a PMT if $\frac{dL(r,\cos(\Theta))}{dr}\Delta r \approx \sigma_t \cdot \frac{c}{n}$ from where:

$$\sigma_r = \frac{c}{n} \frac{\sigma_t(T)}{\frac{dL(r,y)}{dr}}.$$

Summing over all PMTs and substituting the summing with an integration over $y \equiv \cos(\Theta)$, we will obtain

$$\sigma^2_{T_0} = \frac{1}{N_{PM}} [\frac{1}{2} \int_{-1}^{+1} \frac{1 - e^{-\mu F(T(r,y))}}{\sigma^2(T(r,y))} dy]^{-1}. \tag{49}$$

$$(\frac{1}{\sigma_r})^2 = \sum \frac{1}{\sigma_{r_i^2}} \approx N_{PM} \cdot \frac{1}{2} \int_{-1}^{+1} \frac{(\frac{dL(r,y)}{dr})^2}{(\frac{c}{n})^2 \sigma^2_t(T(r,y))} dy \, .$$

Taking into account the relations for $\frac{dL}{dr}$ and $\sigma_t(T)$ we can finally write:

$$\sigma_r(r) = \frac{1}{\sqrt{N_{PM}}}\frac{c}{n}\left[\frac{1}{2}\int_{-1}^{+1}(\frac{r - L_0 \cdot y}{L(r,y)\cdot\sigma_t(T(r,y))})^2(1 - e^{-\mu(r,y)F(T(r,y))})dy\right]^{-1}. \quad (50)$$

The same relation can be obtained for the azimuthal resolution:

$$(\frac{1}{\sigma_\Theta})^2 = \sum\frac{1}{\sigma_{r_i^2}} \approx N_{PM}\cdot\frac{1}{2}\int_{-1}^{+1}\frac{(\frac{1}{r}\frac{dL(r,y)}{dy})^2}{(\frac{c}{n})^2\sigma_t^2(T(r,y))}dy\,,$$

$$\sigma_\Theta(r) = \frac{1}{\sqrt{N_{PM}}}\frac{c}{n}\left[\frac{1}{2}\int_{-1}^{+1}(\frac{L_0 \cdot y}{L(r,y)\cdot\sigma(T)})^2(1 - e^{-\mu(r,y)F(T(r,y))})dy\right]^{-1}. \quad (51)$$

It should be noted that the estimate for the mean time of flight is only approximate due to the simplified geometrical relations used. In the CTF detector for events close to the inner vessel, the refraction effects at the scintillator/water interface will complicate the precise time of flight estimation. Nevertheless, comparison with a precise calculation shows that these effects can be neglected.

4.1.1 Special case: an event at the detector's center.

Let us assume that for an event of an energy E occurred at the detector's center the total registered charge is Q_0 and the mean p.e. number registered by one PMT is $\mu_0 = \frac{Q_0}{N_{PM}}$. Assuming the relative sensitivities of the PMTs to be equal, one can simplify the formula (50) for events at the detector's center:

$$\sigma_x^{(t)} = \sqrt{3}\frac{\frac{c}{n}\sqrt{\sigma^2(T) + \sigma_{T_0}^2(T)}}{\sqrt{N_{PM}(1 - Exp(-\mu_0 F(T))}}, \quad (52)$$

where

$$\begin{aligned}\sigma(T) &= \frac{\int_{T_{min}}^{T}\rho(t)(t - < t(T) >)^2 dt}{F(T)}\\ < t(T) > &= \frac{\int_{T_{min}}^{T}\rho(t)t dt}{F(T)},\\ F(t) &= \int_{T_{min}}^{T}\rho(t)dt\,,\end{aligned}$$

and:

- **n** is the scintillator refraction index;

- $N_{PM}(1-Exp(-\mu_0 F(T)))$ is the mean number of PMTs triggered in the time interval $[T_{min}; T]$ for an event in which the mean number μ_0 of photoelectrons is registered by one PMT;
- T_0 is the moment of scintillation;

The T_{min} parameter here ($T_{min} < T_0$) is chosen to satisfy the relation $\int_{-\infty}^{T_{min}} \rho(t)dt \simeq 0$. The factor $\sqrt{3}$ - appears from the averaging over all PMTs (volume factor).

4.2 Precision of the spatial reconstruction using time data calculated for CTF.

The precision of the spatial reconstruction for CTF is presented in fig.15 as a function of T_{cut}. The time data only are used in the estimations. In order to compare the estimation with real data, only 50 PMTs were considered (as in CTF for the runs with the artificial radon source).

4.3 Precision of the spatial reconstruction using time data calculated for BOREXINO.

The precision of the spatial reconstruction for Borexino is presented in fig.16 as a function of T_{cut}. The time data only are used in the estimations. It should be pointed out that the p.d.f. of the time of arrival of the first photon obtained in the laboratory measurements have been used in the calculations resulting in an overestimate of the reconstruction resolution using the time signals. Nevertheless, the behaviour of the spatial reconstruction precision as a function of T_{cut} is demonstrated.

5 Reconstruction using time and charge signals simultaneously

The reconstruction of an event position is performed using the maximum likelihood method with 5 free parameters: 3 coordinates, one timing parameter τ_1 and the total charge Q. The likelihood function is in this case the sum of the likelihood functions (29) and (41):

$$L(x,y,z,\tau_0,Q_0) = log\left(\prod_{i=1,t_i<T_{max_i}}^{N_{PM}} p\left(\tau(\overrightarrow{r_i}(x,y,z),\tau_0,tdc_i),\ \mu(Q_0,\overrightarrow{r_i}(x,y,z)),\ p_t\right)\right) + \\ + log\left(\prod_{i=1}^{N_{PM}} p\left(\mu(\overrightarrow{r_i}(x,y,z),Q_0),q_i\right)\right). \quad (53)$$

The notations used are the same as in (29) and (41).

One can expect that the precision of reconstruction using (53) can be obtained by summing quadratically the separate resolutions for the reconstruction using the time

Figure 15: The precision of the spatial reconstruction for CTF as a function of T_{cut}. The time data only are used in estimations. Two sources with different energies have been considered at different source distances from the detector's center.

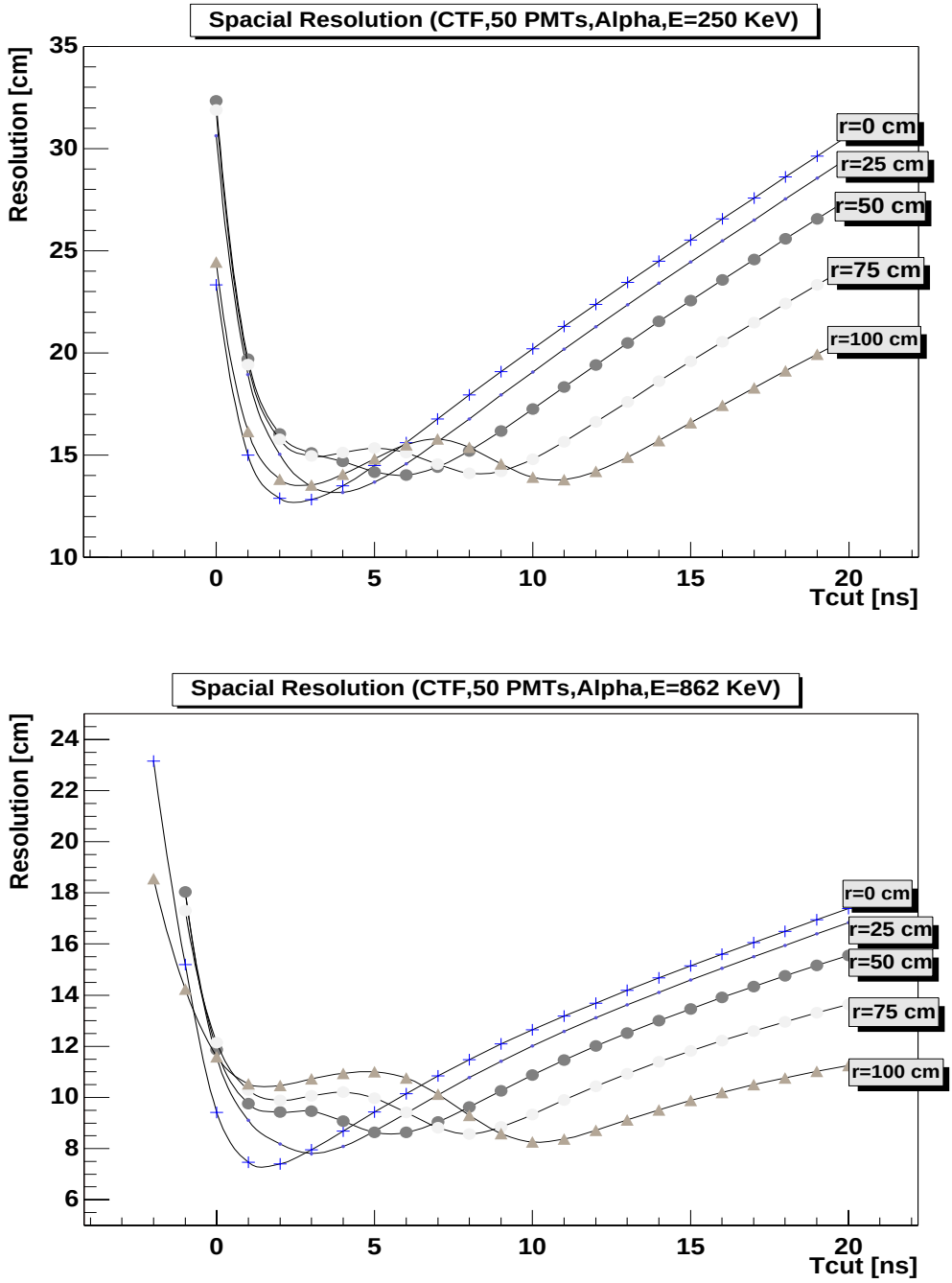

Figure 16: The precision of the spatial reconstruction for Borexino as a function of T_{cut}. The time data only are used in estimations. Two sources with different energies have been considered at different source distances from the detector's center.

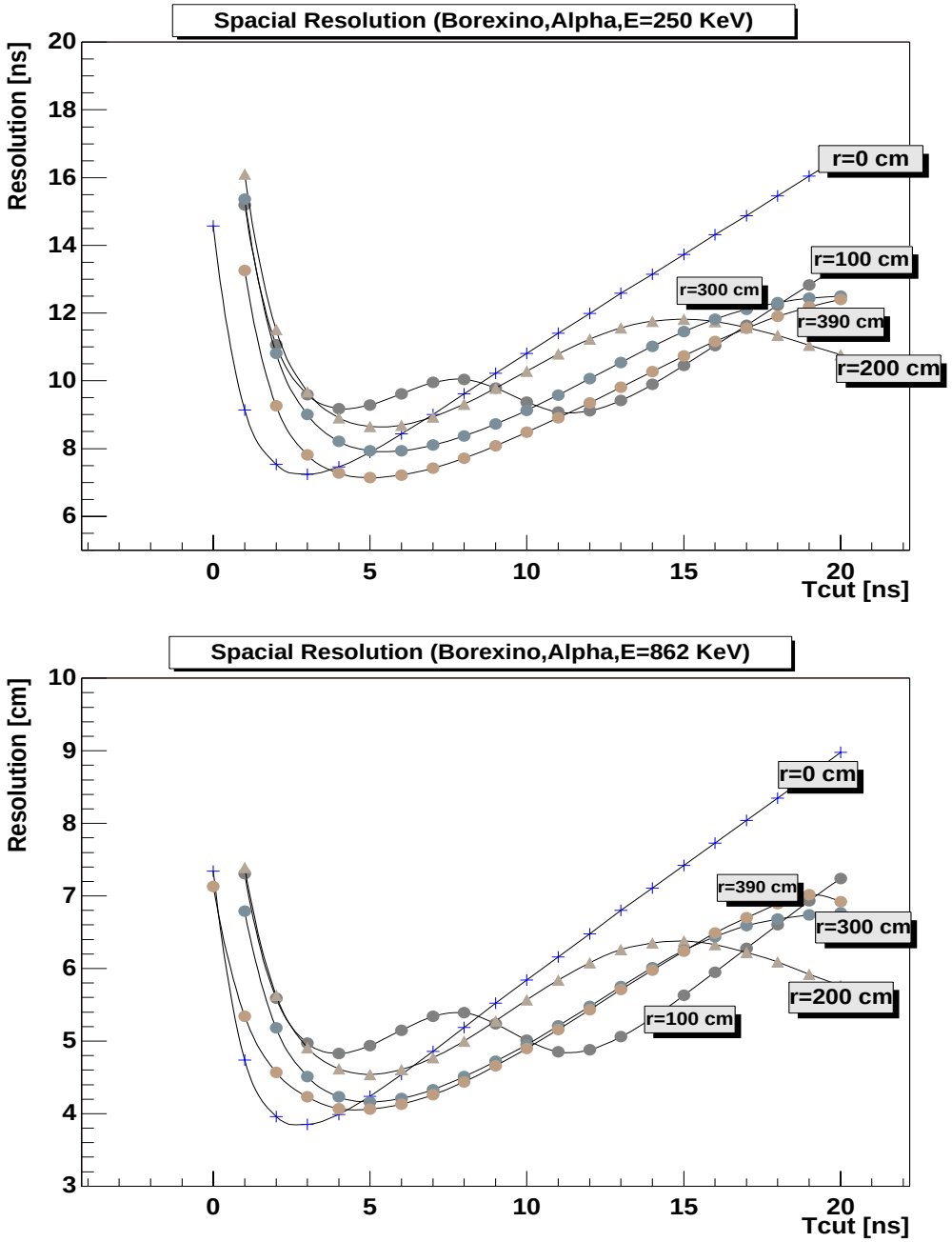

signals and the one using charge signals. Examples of the reconstruction for CTF data are presented in fig.17. One can see a significant improvement of the reconstruction when using both charge and time data.

The reconstructed energy using both charge and time data was presented in fig.8. As it was already pointed out, the combined use of the charge and time data allows better reconstruction of the energy; it is even better than simple correction using the geometrical factor $f_s(r)$.

5.1 Improvement of the spatial reconstruction when using the time and charge data for CTF.

The precision of the spatial reconstruction for CTF is presented in fig.18 as a function of T_{cut}. The time and charge data are used in estimations. These plots should be compared to those in fig.15. In order to compare the estimations to real data, only 50 PMTs were considered (as in CTF for the runs with the radon source). One can see that significant improvement of the resolution can be obtained, especially in the region near the inner vessel boundary. Notice that the resolution at r=75 cm is even better than at the detector's center.

5.2 Improvement of the spatial reconstruction when using the time and charge data for BOREXINO.

The precision of spatial reconstruction for Borexino as a function of T_{cut} is presented in fig.18. These plots should be compared to those in fig.16. The improvement in resolution is not so evident in these plots, but nevertheless one can see that some improvement of the resolution can be obtained in the region near the inner vessel boundary. Notice that the resolution at r=390 cm is comparable to the resolution at the detector's center. As it was already mentioned, in the calculations the "sharp" p.d.f. of the time of arrival of the first photon, obtained in the laboratory measurements, have been used. This caused an overestimation of the reconstruction resolution using the time signals.

6 Acknowledgements

This job would have been impossible without the support from the INFN sez. di Milano. I would like to thank Prof. G.Bellini and Dr. G.Ranucci who organized my stay at the LNGS laboratory.

I would also like to thank the following people: Dr. G.Ranucci who was the first to point out to me the possibility to use charge signals from the PMTs for the spatial reconstruction. Prof. O.Zaimidoroga for useful discussions and support. Also, of course, all my colleagues from the Borexino collaboration. Special thanks to A.Ianni, G.Korga, L.Papp, R.Ford, R.Scardaoni for their friendliness. I am very grateful to Richard Ford for the careful reading of the manuscript and really useful discussions.

Figure 17: Example of the reconstruction using the time and charge data with CTF data. The artificial radon source is at the position r(4,-63,76)=98 cm from the detector's center. The upper plot presents the reconstruction of the source position using charge only (red dashed lines) and time only (black solid lines) data. The central plot presents the reconstruction of the source position using charge and time (red dashed lines) and time only (black solid lines) data. In the lower plot the reconstructed distance from the nominal source position is presented. The first plot shows charge only and time data only reconstruction. The last one shows the reconstruction using charge and time data (red narrow plot) in comparison to the time data only reconstruction (black wider plot).

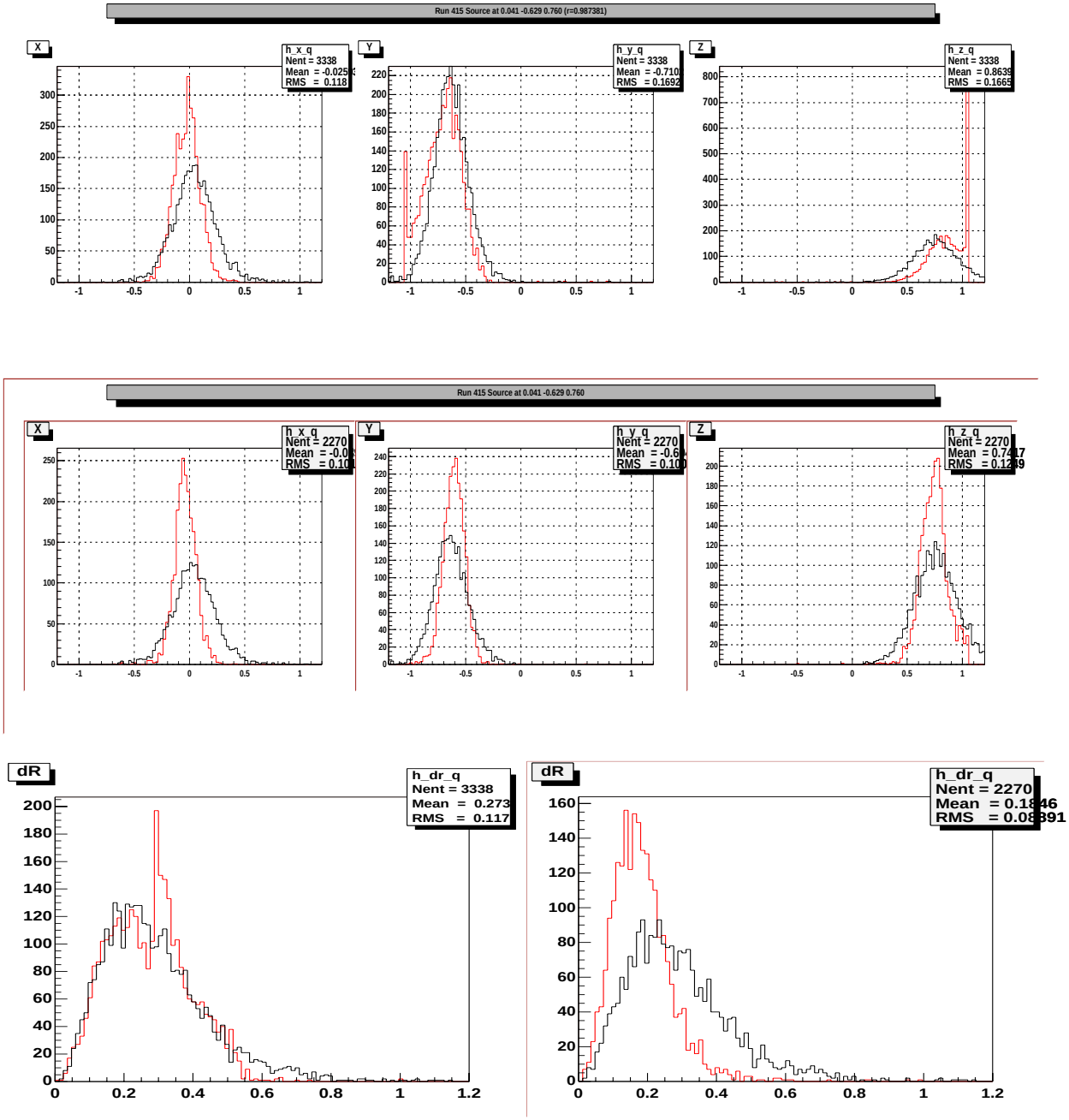

Figure 18: The precision of the spatial reconstruction precision for CTF as a function of T_{cut} .The time and charge data are used in estimations. Two sources with different energies have been considered at different source distances from the detector's center.

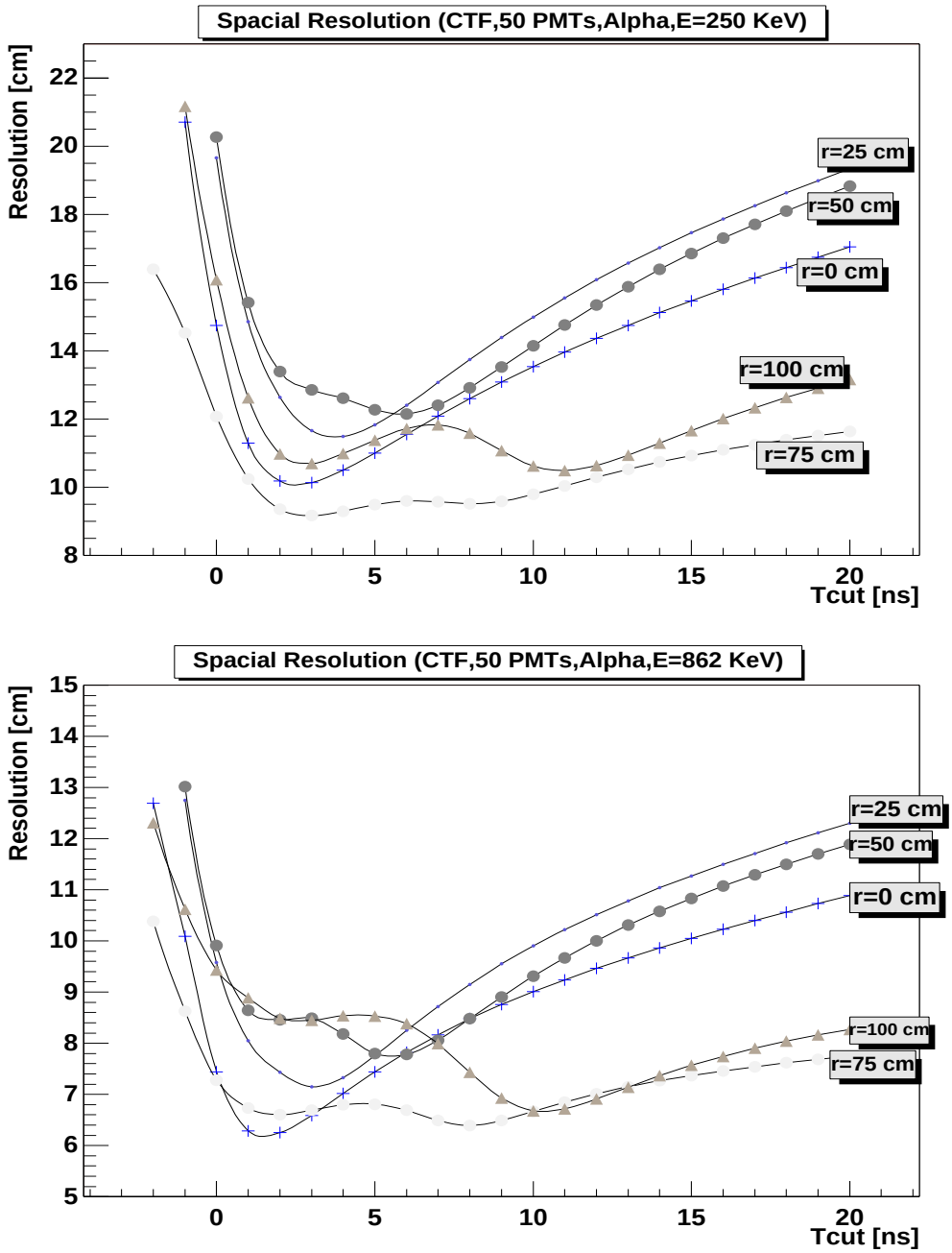

Figure 19: The precision of the spatial reconstruction for Borexino using charge and time data as a function of T_{cut} .The time and charge data are used in estimations. Two sources with different energies has been considered at the different source distance from the detector's center.

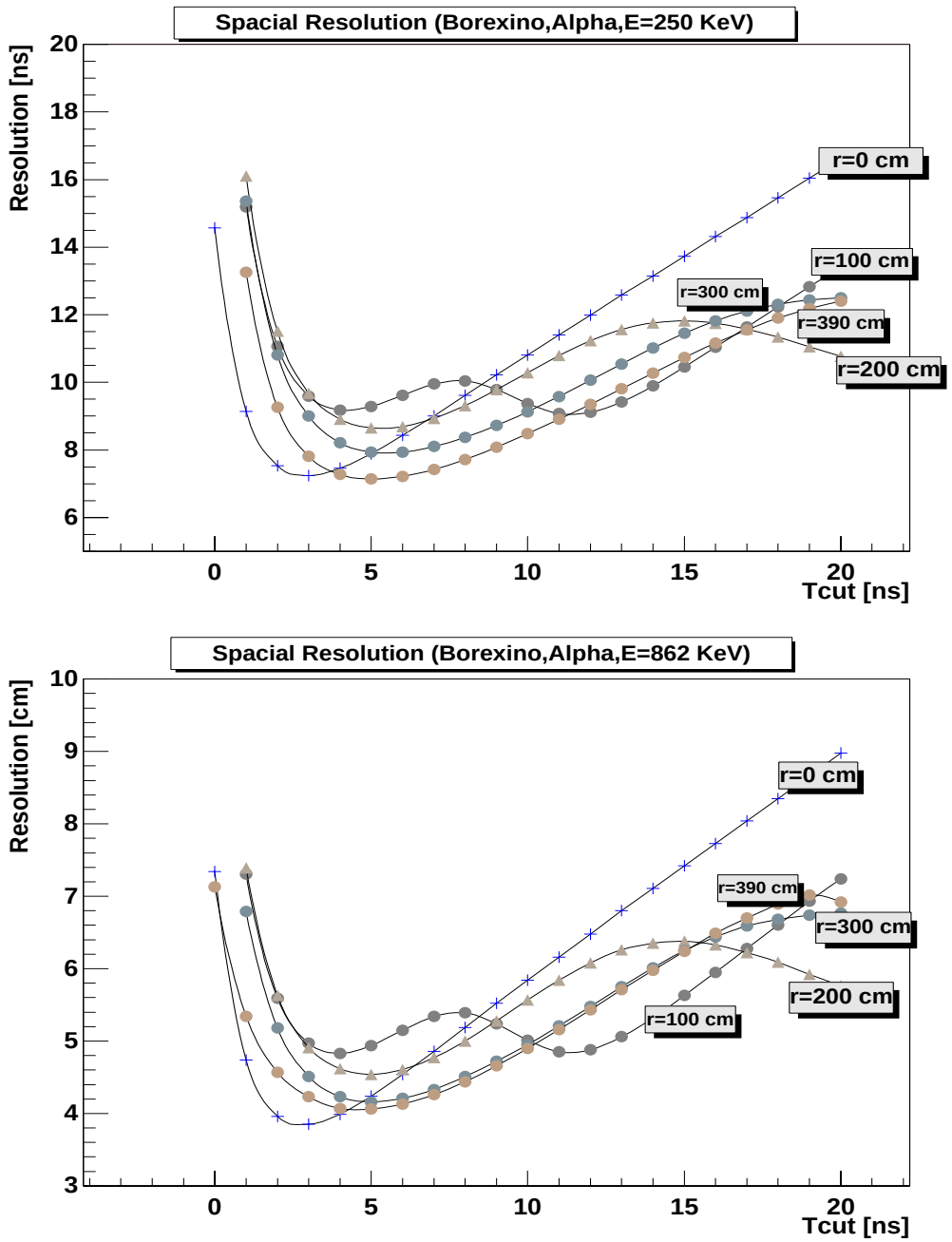

References

[1] J.B. Birks, The Theory and Practice of Scintillation Counting (Macmillan, New York, 1964).

[2] Arpesella C. et al
Borexino at Gran Sasso - Proposal for a real time detector for low energy solar neutrino.. Volume 1.
Edited by G.Bellini,M.Campanella,D.Guigni.
Dept. of Physics of the University of Milano. August 1991.

[3] Alimonti G. et al
A large scale low-background liquid scintillator detector: the counting test facility at Gran Sasso
NIM A 406 (1998) p.411-426.

[4] Alimonti G., et al
Light propagation in a large volume liquid scintillator.
NIM A440 (1998) 360.

[5] R. Dossi, A. Ianni, G. Ranucci, O. Ju. Smirnov
Methods for precise photoelectron counting with photomultipliers.
INFN/TC-98/18, July 17 1998. (to appear in NIM A).

[6] M. Johnson, J. Benziger, C. Stoia, F. Calaprice, M. Chen, N. Darnton, F. Loeser, R. Bruce Vogelaar
A ^{222}Rn Source for Low-background Liquid Scintillation Detectors.
NIM A414 (1998) 459.

[7] G. Ranucci *et al.*, "Scintillation decay time and pulse shape discrimination of binary organic liquid scintillators for the Borexino detector",NIM A350 (1994) 338;